Computational Methods and Function Theory
Volume 11 (2011), No. 2, 747–787

Numerical Computation of Surface Conformal Mappings

Xianfeng David Gu, Wei Zeng, Feng Luo and Shing-Tung Yau

(Communicated by Thomas K. DeLillo)

Abstract. We report recent progress in the computation of conformal mappings from surfaces with arbitrary topologies to canonical domains. Two major computational methodologies are emphasized; one is holomorphic differentials based on Riemann surface theory and the other is surface Ricci flow from geometric analysis. The applications of surface conformal mapping in the field of engineering are briefly reviewed.

Keywords. Conformal geometry, Ricci flow, holomorphic differential, discrete surface.

2000 MSC. Primary 53A30; Secondary 52C26.

1. Introduction

Conformal mapping plays an important role in mathematics and engineering. Historically, planar conformal mapping has been broadly applied in many engineering fields [57], such as electro-magnetics, vibrating membranes and acoustics, elasticity, heat transfer and fluid flow. Recently, with the development of 3D scanning technology, increasing of computational power, and further advances in mathematical theories, surface conformal mapping has been developed greatly and applied in computer graphics, medical imaging, computer vision, geometric modeling and networking fields. This work focuses on numerical computation of surface conformal mappings; our methods are based on Hodge theory and surface Ricci flow.

Received June 21, 2011, in revised form August 16, 2011.
Published online October 12, 2011.
The research has been supported by NSF CCF-0448399, NSF DMS-0528363, NSF DMS-0626223, NSF IIS-0713145, NSF CCF-0830550, NSF CCF-0841514, ONR N000140910228, NSF III 0916286, NSF CCF-1081424, NSF Nets 1016829, NIH R01EB7530, and NSFC 60628202.

ISSN 1617-9447/$ 2.50

1.1. Surface conformal mappings. Let S_1 and S_2 be two surfaces with Riemannian metrics $\mathbf{g}_1$, $\mathbf{g}_2$, and $\phi\colon (S_1, \mathbf{g}_1) \to (S_2, \mathbf{g}_2)$ be a diffeomorphism between them. We say ϕ is *conformal* if the pull back metric induced by ϕ is proportional to the original metric $\mathbf{g}_1$

$$\phi^* \mathbf{g}_2 = e^{2\lambda} \mathbf{g}_1.$$

A conformal map preserves angles, as shown in Figure 1.

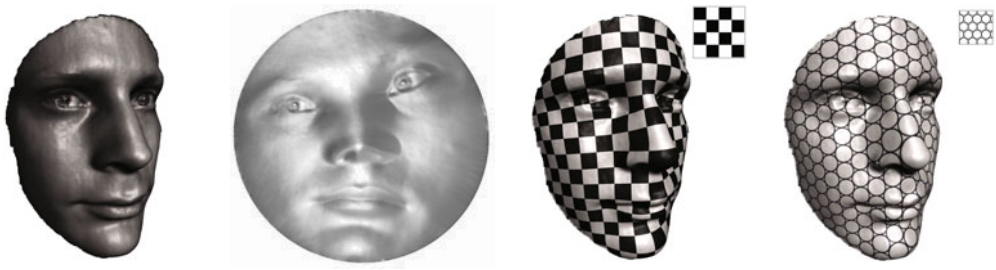

FIGURE 1. Conformal mappings preserve angles and infinitesimal circles.

Infinitesimally, a conformal mapping is a scaling and rotation transformation; it preserves local shapes. For example, it maps infinitesimal circles to infinitesimal circles. As shown in Figure 1, if a circle packing is given on the plane and pulled back by ϕ, it produces a circle packing on the face surface; if a checkerboard is given on the plane, then pulled back by ϕ, the checkerboard pattern on the face surface is such that all the right angles of the squares are preserved.

All Riemann surfaces can be unified by the following theorem:

Theorem 1.1 (Poincaré-Klein-Koebe uniformization [22, p. 206])**.** *Every connected Riemann surface S is conformally equivalent to D/G with where D is one of the three canonical spaces:*

(i) *extended complex plane $\mathbb{C} \cup \{\infty\}$;*
(ii) *complex plane $\mathbb{C}$;*
(iii) *unit disk $D = \{z \in \mathbb{C}\colon |z| < 1\}$*

where G is a subgroup of Möbius transformations that acts freely discontinuous on D. Furthermore, $G \cong \pi_1(S)$, where $\pi_1(S)$ is the fundamental group of S.

Definition 1.2 (Circle domain)**.** A circle domain in a Riemann surface is a domain such that the components of the complement of the domain are closed geodesic disks and points. Here a geodesic disk in a Riemann surface is a topological disk whose lift in the universal cover is a round disk in $\mathbb{S}^2$, $\mathbb{E}^2$ or $\mathbb{H}^2$.

Theorem 1.3 (He and Schramm [36, Thm. 0.1])**.** *Let S be an open Riemann surface with finite genus and at most countably many ends. Then there is a closed Riemann surface $\tilde{S}$, such that S is conformally homeomorphic to a circle domain Ω in $\tilde{S}$. Moreover, the pair $(\tilde{S}, \Omega)$ is unique up to conformal homeomorphisms.*

The uniformization theorem states that the universal covering space of closed metric surfaces can be conformally mapped to one of three canonical spaces, the sphere $\mathbb{S}^2$, the plane $\mathbb{E}^2$, or the hyperbolic space $\mathbb{H}^2$, as shown in Figure 2. Similarly, uniformization theorem holds for surfaces with boundaries as shown in Figure 3, the covering space can be conformally mapped to a circle domain in $\mathbb{S}^2$, $\mathbb{E}^2$ or $\mathbb{H}^2$.

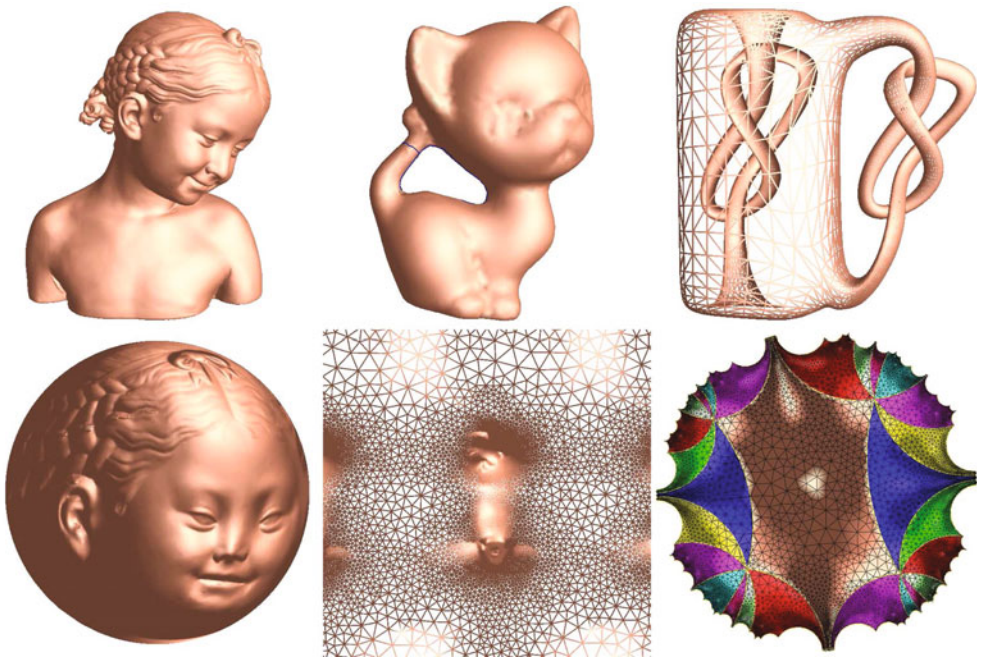

FIGURE 2. Uniformization for closed surfaces. The universal covering space of an oriented closed metric surface can be conformally mapped to one of the three canonical shapes: the unit sphere, the Euclidean plane or the hyperbolic space.

1.2. Computational strategies. There are three major approaches for surface conformal mappings. The first one is based on surface Ricci flow, the second one is based on holomorphic differentials using Hodge theory, and the third one is based on harmonic mapping using non-linear heat flow.

Ricci flow. Suppose we want to find a conformal mapping between two metric surfaces $\phi\colon (S_1, \mathbf{g}_1) \to (S_2, \mathbf{g}_2)$. Then the pull back metric induced by ϕ is $\phi^* \mathbf{g}_2 = e^{2u} \mathbf{g}_1$, where $uc\colon S_1 \to \mathbb{R}$ is the unknown conformal factor function, satisfying the following Yamabe equation

$$K_2(\phi(p)) = \frac{1}{e^{2u(p)}}[K_1(p) - \Delta_{\mathbf{g}_1}(u(p))], \qquad p \in S_1,$$

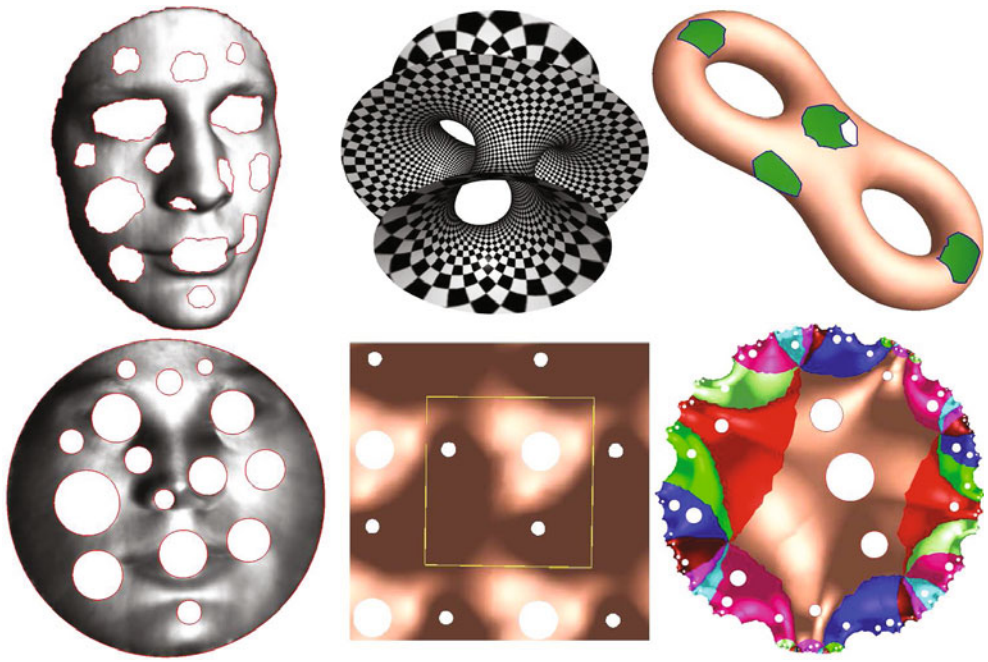

FIGURE 3. Uniformization for surfaces with boundaries. The covering space of an oriented metric surface with boundaries can be conformally mapped to one of the three canonical shapes: the unit sphere, the Euclidean plane or the hyperbolic space, and all the boundaries are mapped to geodesic circles.

where K_1, K_2 are the Gaussian curvatures induced by $\mathbf{g}_1$ and $\mathbf{g}_2$, and $\Delta_{\mathbf{g}_1}$ is the Laplace-Beltrami operator induced by $\mathbf{g}_1$. By solving the Yamabe equation, the conformal factor u can be obtained, and then the mapping ϕ can be found. The Yamabe equation can be solved directly by surface Ricci flow:

$$\frac{du}{dt} = K_2 - K_1.$$

Holomorphic differential. Suppose the target surface $(S_2, \mathbf{g}_2)$ is a region on the complex plane $\mathbb{C}$, or a quotient space of $\mathbb{C}$, then dz is a holomorphic 1-form on S_2. The pull back complex differential form $\omega = \phi^* dz$ is a holomorphic 1-form on $(S_1, \mathbf{g}_1)$. All the holomorphic 1-forms on S_1 form a group $\Omega^{1,0}$. We can compute the basis of this group, then find the appropriate 1-form $\omega = \phi^* dz$ in $\Omega^{1,0}$, and construct the mapping ϕ by integrating ω on S_1.

Spherical harmonic maps. Harmonic maps between two surfaces minimize the harmonic energy. For genus zero closed surfaces, harmonic maps are conformal. All genus zero closed surfaces can be conformally mapped to the unit sphere; two such kinds of mapping differ by a Möbius transformation. We can

use the non-linear heat flow method to diffuse a degree one map to a harmonic map with special normalization to a conformal map.

1.3. Outline. The work is organized as follows: Section 2 briefly reviews existing works most related to the current one. Section 3 introduces the computational methods: surface Ricci flow, holomorphic differential form and harmonic map. Section 4 explains the algorithms for computing conformal moduli and conformal mappings using methods in Section 3. The last section demonstrates the applications of conformal geometric methods in several engineering fields, such as computer graphics, geometric modeling, medical imaging, computer vision, and wireless sensor networks.

2. Previous work

Computational conformal geometry is an inter-disciplinary field, and has a long history. Researchers in mathematics, physics, medicine, computer science and many other engineering fields have made great contributions to the subject. A thorough literature review is beyond the scope of this work. In the following, we briefly review only the most relevant work. Most conformal geometric methods are for planar domains or topological disks (genus zero surface with a single boundary), whereas our current work focuses on methods for surfaces with complicated topologies. Therefore, many important works for planar domains or topological disks may be skipped due to the page limit.

2.1. Planar domains. Conventional computational complex analysis methods focus on conformal mappings on planar domains. Thorough surveys can be found in [37, 17, 40, 3, 65, 68]. Schwarz-Christoffel Mapping has been broadly applied for computing Riemann mappings, such as in [20, 2]. Schwarz-Christoffel mapping of multiply connected domains can be found in [18, 15]. Recently, a geodesic zipper algorithm based on iterating simple maps has been introduced in [51], and a linear conformal mapping algorithm based on hyperbolic geometry can be found in [4]. A robust algorithm based on cross ratio and Delaunay triangulation can be found in [21]. Circle packing methods lead to the theory of discrete analytic functions [60], which is one of the few planar methods that has actually been used for surface maps.

2.2. Genus zero surfaces. In the computer graphics field, there is vast research on computing conformal mappings, mainly for surfaces with disk topology. Discrete harmonic maps were constructed in [53], where the cotan formula was introduced. First order finite element approximations of the Cauchy-Riemann equations were introduced by Levy et al. [49]. Discrete intrinsic parameterization by minimizing Dirichlet energy was introduced by [19]. Mean value coordinates were introduced in [23] to compute generalized harmonic maps. Conformal mappings for topological spheres are discussed in [27, 31]. In the computer graphics

field, thorough surveys on surface conformal mappings for topological disks or topological spheres can be found in [24, 45].

2.3. High genus surfaces. Two major approaches for computing the conformal structures of high genus surfaces are *holomorphic differentials* and *discrete curvature flow*.

Holomorphic differential. Discrete holomorphic forms are introduced by Gu and Yau [29] to compute global conformal structure for high genus surfaces. The method is based on Hodge theory and uses the heat diffusion method to compute harmonic forms in each cohomology class. All the computations are carried out on discrete polyhedral surfaces. A different approach for constructing the discrete Hodge star operator can be found in [53] for computing minimal surfaces. Another approach of discrete holomorphy was introduced in [52] by discretization of the Cauchy-Riemann equation. The method requires regular connectivity of the mesh. General discrete exterior calculus was presented in [38].

Gortler et al. [26] used the discrete 1-form to parameterize genus one meshes [61]. Tong et al. [64] generalized the 1-form method to incorporate cone singularities, and applied the method for remeshing and tiling. The holomorphic differential method has been applied to compute conformal mappings of genus zero surfaces with multiple boundaries in [77]. Quasi-conformal mapping based on holomorphic differentials can be found in [74].

Surface Ricci flow. Ricci flow was introduced by R. Hamilton in a seminal paper [35] for Riemannian manifolds of any dimension. Ricci flow has revolutionized the study of the geometry of surfaces and 3-manifolds and has inspired a lot of research in geometry. In particular, it makes possible a proof of the 3-dimensional Poincaré conjecture. In the paper [34], Hamilton used the 2-dimensional Ricci flow to give a proof of the uniformization theorem for surfaces of positive genus. This leads the way for potential applications in computer graphics.

There are many ways to discretize smooth surfaces. The one which is particularly related to a discretization of conformality is the circle packing metric introduced by Thurston [62]. The notion of circle packing has appeared in the work of Koebe [44]. Thurston conjectured in [63] that for a discretization of the Jordan domain in the plane, the sequence of circle packings converge to the Riemann mapping. This was proved by Rodin and Sullivan [54].

Colin de Verdiere [11] established the first variational principle for circle packing and proved Thurston's existence of circle packing metrics. This paved a way for a fast algorithmic implementation of finding the circle packing metrics, such as the one by Collins and Stephenson [13]. In [10], Chow and Luo generalized Colin de Verdiere's work and introduced the discrete Ricci flow and discrete Ricci energy on surfaces. They proved a general existence and convergence theorem for the

discrete Ricci flow and proved that the Ricci energy is convex. The algorithmic implementation of the discrete Ricci flow was carried out by Jin et al. [41].

Another related discretization method is called circle pattern; it considers both the combinatorics and the geometry of the original mesh, and can be regarded as a variant to circle packings. Circle pattern was proposed by Bowers and Hurdal [7], and has been proven to be a minimizer of a convex energy by Bobenko and Springborn [5]. An efficient circle pattern algorithm was developed by Kharevych et al. [43].

Yamabe flow on surfaces. The Yamabe problem aims at finding a conformal metric with constant scalar curvature for compact Riemannian manifolds. The first proof (with flaws) was given by Yamabe [69] and was corrected and extended to a complete proof by several researchers including Trudinger [66], Aubin [1] and Schoen [58]. A comprehensive survey of this topic was given by Lee and Parker in [48].

In [50] Luo studied the discrete Yamabe flow on surfaces. He introduced a notion of discrete conformal change of polyhedral metric, which plays a key role in developing the discrete Yamabe flow and the associated variational principle in the field. Based on the discrete conformal class and geometric consideration, Luo gave the discrete Yamabe energy as an integration of a differential 1-form and proved that this energy is a locally convex function. He also deduced from it that the curvature evolution of the Yamabe flow is a heat equation.

Another recent work by Gu et al. [30], which used the original discrete Yamabe energy from [50], has produced an equally efficient algorithm for finding the discrete conformal metrics. In addition, discrete hyperbolic Yamabe flow was discussed in [6]. It is applied for computing hyperbolic structure and the canonical homotopy class representative in [72].

3. Computational methods

In this section, we briefly introduce the major computational methods. In the next section, we will apply these methods for computing conformal mappings for surfaces with different topologies.

3.1. Surface Ricci flow. Surface Ricci flow is a powerful tool to construct conformal Riemannian metrics with prescribed Gaussian curvatures. Discrete surface Ricci flow generalizes the curvature flow method from smooth surfaces to discrete triangular meshes. The key insight to discrete Ricci flow is based on the following observation: conformal mappings transform infinitesimal circle fields to infinitesimal circle fields. Discrete Ricci flow replaces infinitesimal circles by circles with finite radii, and modifies the circle radii to deform the discrete metric, to achieve the desired curvature.

Classical surface Ricci flow.

Definition 3.1 (Isothermal coordinates)**.** Let S be a smooth surface with a Riemannian metric $\mathbf{g}$. Isothermal coordinates $z = u + iv$ for $\mathbf{g}$ satisfy

$$\mathbf{g} = e^{2\lambda(u,v)}(du^2 + dv^2) = e^{2\lambda(z)}dzd\bar{z}.$$

Locally, isothermal coordinates always exist [8]. An atlas with all local coordinates being isothermal is a conformal atlas, such that all the chart transition functions are bi-holomorphic.

The Gaussian curvature of the surface is given by

$$K(u,v) = -\Delta_{\mathbf{g}}\lambda, \tag{1}$$

where

$$\Delta_{\mathbf{g}} = e^{-2\lambda(u,v)}\left(\frac{\partial^2}{\partial u^2} + \frac{\partial^2}{\partial v^2}\right)$$

is the Laplace-Beltrami operator induced by $\mathbf{g}$. Although the Gaussian curvature is intrinsic to the Riemannian metric, the total Gaussian curvature is a topological invariant according to the Gauss-Bonnet theorem:

$$\int_S K\,dA = 2\pi\chi(S), \tag{2}$$

where $\chi(S)$ is the Euler number of the surface.

Suppose $\mathbf{g}_1$ and $\mathbf{g}_2$ are two Riemannian metrics on the smooth surface S, and they induce Gauss curvatures K_1 and K_2, respectively. If there is a differential function $\lambda\colon S \to \mathbb{R}$, such that

$$\mathbf{g}_2 = e^{2\lambda}\mathbf{g}_1,$$

then the following *Yamabe equation* holds

$$K_2 = \frac{1}{e^{2\lambda}}\left(K_1 - \Delta_{\mathbf{g}_1}\lambda\right).$$

The Yamabe equation can be solved by Hamilton's Ricci flow. For a metric $\mathbf{g} = (g_{ij})$ given in local coordinates, Hamilton's Ricci flow is

$$\frac{dg_{ij}}{dt} = -Kg_{ij}.$$

During the flow, the Gaussian curvature will evolve according to a heat diffusion process.

Theorem 3.2 (Hamilton and Chow [9, Thm. B.1, p. 504])**.** *Suppose S is a closed surface with a Riemannian metric. Then the normalized Ricci flow will converge to a Riemannian metric of constant Gaussian curvature.*

Background geometry. In engineering fields, smooth surfaces are approximated by polyhedral surfaces, namely, a triangle mesh.

Definition 3.3 (Triangle mesh)**.** A triangle mesh Σ is a 2 dimensional simplicial complex, which is homeomorphic to a surface.

It is generally assumed that a mesh Σ is embedded in the three dimensional Euclidean space $\mathbb{R}^3$, and therefore each face is Euclidean. In this case, we say the mesh is with Euclidean background geometry. Similarly, we can assume that a mesh is embedded in the three dimensional sphere $\mathbb{S}^3$ or hyperbolic space $\mathbb{H}^3$, then each face is a spherical or a hyperbolic triangle. We say the mesh is with spherical or hyperbolic background geometry.

Discrete Riemannian metric. A discrete Riemannian metric on a mesh Σ is a piecewise constant curvature metric with cone singularities at the vertices. The edge lengths are sufficient to define a discrete Riemannian metric,

$$l\colon E \to \mathbb{R}^+, \tag{3}$$

as long as, for each face $[v_i, v_j, v_k]$, the edge lengths satisfy the triangle inequality: $l_{ij} + l_{jk} > l_{ki}$ for all the three background geometries, and another inequality: $l_{ij} + l_{jk} + l_{ki} < 2\pi$ for spherical geometry.

Cosine laws. In the smooth case, the curvatures are determined by the Riemannian metrics as in (1). In the discrete case, the angles of each triangle are determined by the edge lengths. According to different background geometries, there are different cosine laws. For simplicity, we use e_i to denote the edge across from the vertex v_i, namely $e_i = [v_j, v_k]$, and l_i the edge length of e_i. The cosine laws are given as:

$$\begin{aligned} {l_k}^2 &= {l_i}^2 + {l_j}^2 - 2l_i l_j \cos\theta_k, && \mathbb{E}^2, \\ \cosh l_k &= \cosh l_i \cosh l_j - \sinh l_i \sinh l_j \cos\theta_k, && \mathbb{H}^2, \\ \cos l_k &= \cos l_i \cos l_j - \sin l_i \sin l_j \cos\theta_k, && \mathbb{S}^2. \end{aligned} \tag{4}$$

Discrete Gaussian curvature. The discrete Gaussian curvature K_i at a vertex $v_i \in \Sigma$ can be computed as the angle deficit,

$$K_i = \begin{cases} 2\pi - \displaystyle\sum_{[v_i,v_j,v_k]\in\Sigma} \theta_i^{jk}, & v_i \notin \partial\Sigma, \\ \pi - \displaystyle\sum_{[v_i,v_j,v_k]\in\Sigma} \theta_i^{jk}, & v_i \in \partial\Sigma, \end{cases} \tag{5}$$

where θ_i^{jk} represents the corner angle attached to vertex v_i in the face $[v_i, v_j, v_k]$, and $\partial\Sigma$ represents the boundary of the mesh.

Discrete Gauss-Bonnet Theorem. The Gauss-Bonnet Theorem (2) states that the total curvature is a topological invariant. It still holds on meshes as follows.

$$\sum_{v_i \in V} K_i + \lambda \sum_{f_i \in F} A_i = 2\pi\chi(M), \tag{6}$$

where the second term is the integral of the ambient constant Gaussian curvature on the faces; A_i denotes the area of face f_i, and λ represents the constant curvature for the background geometry: $+1$ for the spherical geometry, 0 for the Euclidean geometry, and -1 for the hyperbolic geometry.

Discrete conformal metric deformation. In the smooth case, *Conformal deformation of a Riemannian metric* is defined as

$$\mathbf{g} \mapsto e^{2\lambda}\mathbf{g}, \quad \lambda \colon S \to \mathbb{R}. \tag{7}$$

In the discrete case, there are many ways to define conformal metric deformation. Figure 4 illustrates some of them.

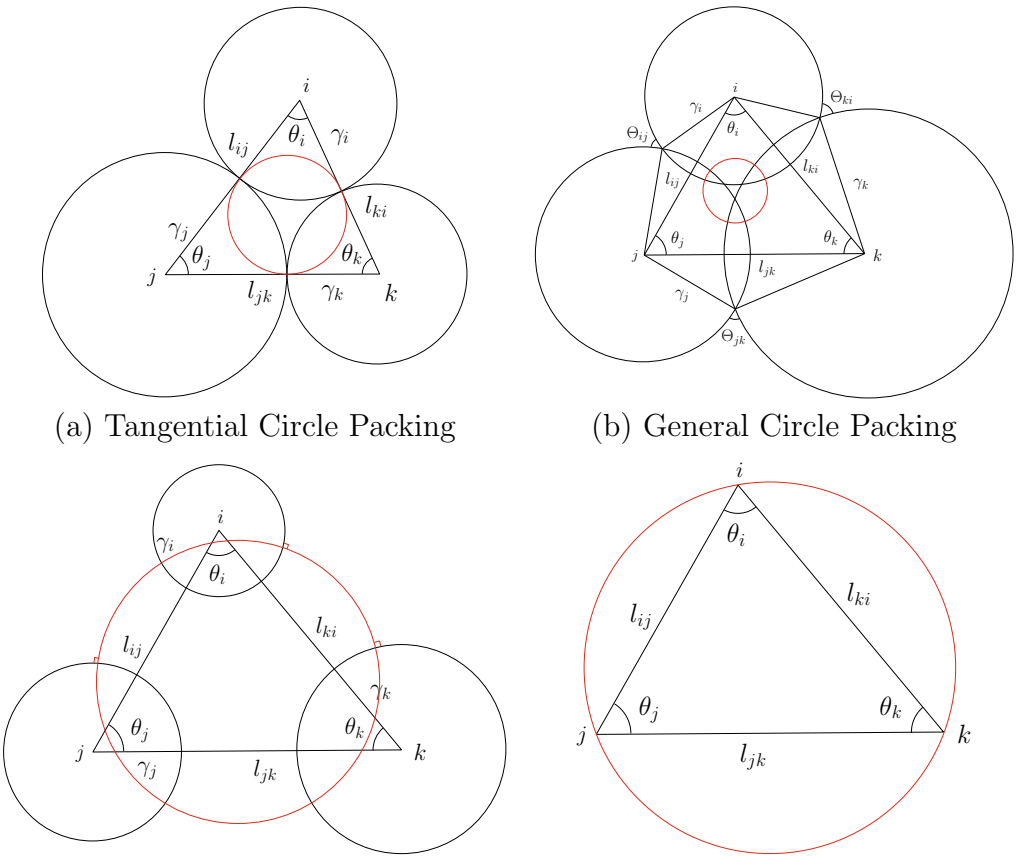

(a) Tangential Circle Packing (b) General Circle Packing

(c) Inversive Distance Circle Packing (d) Combinatorial Yamabe flow

FIGURE 4. Different configurations for discrete conformal metric deformation.

Generally, we associate each vertex v_i with a circle (v_i, γ_i) centered at v_i with radius γ_i. On an edge $[v_i, v_j]$, two circles intersect at an angle Θ_{ij}. During the conformal deformation, the radii of circles can be modified, but the intersection angles are preserved. Geometrically, the discrete conformal deformation can be interpreted as follows [25]: see Figure 5, there exists a unique circle, the so called

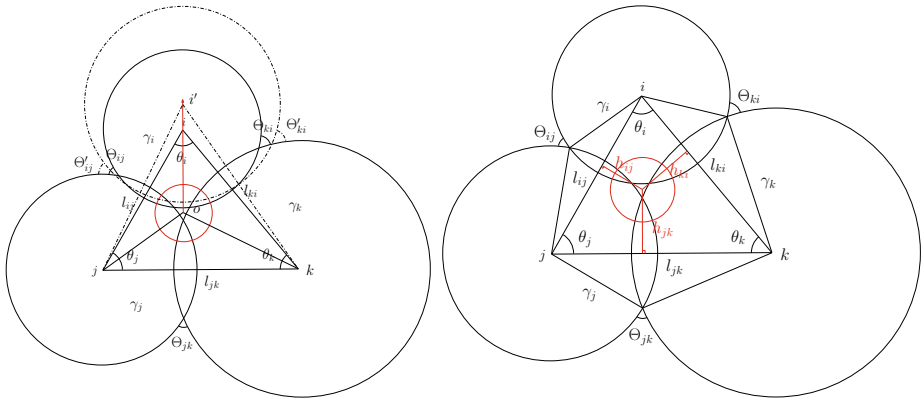

FIGURE 5. Geometric interpretation of discrete conformal metric deformation.

radial circle, that is orthogonal to three vertex circles. The radial circle center is denoted as o. We connect the radial circle center to three vertices, to get three rays $\overrightarrow{ov_i}, \overrightarrow{ov_j}$ and $\overrightarrow{ov_k}$. We deform the triangle by infinitesimally moving the vertex v_i along $\overrightarrow{ov_i}$ to ov'_i, and construct a new circle (v'_i, γ'_i), such that the intersection angles among the circles are preserved, $\Theta'_{ij} = \Theta_{ij}$, $\Theta'_{ki} = \Theta_{ki}$.

The discrete conformal metric deformation can be generalized to all other configurations, with different circle intersection angles (including zero or virtual angles), and different circle radii (including zero radii). In Figure 4, the radial circle is well defined for all cases, as are the rays from the radial circle center to the vertices. Therefore, discrete conformal metric deformations are well defined as well. The precise analytical formulae for discrete conformal metric deformation are explained as follows: let $u\colon V \to \mathbb{R}$ be the *discrete conformal factor*, which measures the local area distortion. If the vertex circles are with finite radii, then u_i can be formulated as

$$u_i = \begin{cases} \log \gamma_i, & \mathbb{E}^2, \\ \log \tanh \dfrac{\gamma_i}{2}, & \mathbb{H}^2, \\ \log \tan \dfrac{\gamma_i}{2}, & \mathbb{S}^2. \end{cases} \tag{8}$$

(i) *Tangential Circle Packing* Figure 4 (a), the intersection angles are 0's. Therefore, the edge length is given by

$$l_{ij} = \gamma_i + \gamma_j,$$

for both the Euclidean case and the hyperbolic case, e.g. [13].

(ii) *General Circle Packing* Figure 4 (b), the intersection angles are acute, $\Theta_{ij} \in (0, \pi/2)$. The edge length is

$$l_{ij} = \sqrt{{\gamma_i}^2 + {\gamma_j}^2 + 2\gamma_i\gamma_j \cos\Theta_{ij}}$$

for the Euclidean case, and

$$l_{ij} = \cosh^{-1}\left(\cosh\gamma_i \cosh\gamma_j + \sinh\gamma_i \sinh\gamma_j \cos\Theta_{ij}\right)$$

in hyperbolic geometry, e.g. [10, 41].

(iii) *Inversive Distance Circle Packing* In Figure 4 (c), all the circles intersect at "virtual" angles. The $\cos\Theta_{ij}$ is replaced by the so-called *inversive distance* I_{ij}, during the deformation, I_{ij}'s are never changed. The edge lengths are given by

$$l_{ij} = \sqrt{{\gamma_i}^2 + {\gamma_j}^2 + 2\gamma_i\gamma_j I_{ij}}$$

for the Euclidean case, and

$$l_{ij} = \cosh^{-1}(\cosh\gamma_i \cosh\gamma_j + \sinh\gamma_i \sinh\gamma_j I_{ij})$$

in hyperbolic geometry, e.g. [33, 70].

(iv) *Combinatorial Yamabe Flow* Figure 4 (d), all the circles are degenerated to points, $\gamma_i = 0$. The discrete conformal factor is still sensible. The edge lengths are given by

$$l_{ij} = e^{u_i} e^{u_j} l^0_{ij},$$

in Euclidean background geometry, e.g. [50], and

$$\sinh\frac{l_{ij}}{2} = e^{u_i} \sinh\frac{l^0_{ij}}{2} e^{u_j},$$

in hyperbolic background geometry, e.g. [6, 72], where l^0_{ij} is the initial edge length of $[v_i, v_j]$.

Admissible metric space. In the following, we want to clarify what we mean by the spaces of all possible metrics and all possible curvatures of a discrete surface.

Let the vertex set be $V = \{v_1, v_2, \ldots, v_n\}$. We represent a discrete metric on Σ by a vector $\mathbf{u} = (u_1, u_2, \ldots, u_n)^T$. Similarly, we represent the Gaussian curvatures at mesh vertices by the curvature vector $\mathbf{k} = (K_1, K_2, \ldots, K_n)^T$. All the possible $\mathbf{u}$'s form the *admissible metric space*, and all the possible $\mathbf{k}$'s form the *admissible curvature space*.

According to the Gauss-Bonnet Theorem (see (6)), the total curvature must be $2\pi\chi(\Sigma)$, and therefore the curvature space is $n-1$ dimensional. We add one linear constraint to the metric vector $\mathbf{u}$, $\sum u_i = 0$, for the normalized metric. As a result, the metric space is also $n-1$ dimensional. For the circle packing metric, if all the intersection angles are acute including zero, then the edge lengths induced

by a circle packing satisfy the triangle inequality. There is no further constraint on $\mathbf{u}$. Therefore, the admissible metric space is simply $\mathbb{R}^{n-1}$.

A curvature vector $\mathbf{k}$ is *admissible* if there exists a metric vector $\mathbf{u}$, which induces $\mathbf{k}$. The admissible curvature space is a convex polytope. The detailed proof can be found in [10]. The admissible curvature space for weighted meshes with hyperbolic or spherical background geometries is more complicated. We refer the readers to [10] for a detailed discussion.

Unfortunately, admissible metric spaces for inversive distance circle packing with both Euclidean and hyperbolic background geometries are non-convex. The admissible metric spaces for the combinatorial Yamabe flow with both Euclidean and hyperbolic background geometries are non-convex.

For tangential and general circle packing cases with both $\mathbb{E}^2$ and $\mathbb{H}^2$ background geometries, see Figure 4 (a) and (b), the correspondence between the curvature $\mathbf{k}$ and metric $\mathbf{u}$ is globally one-to-one. This is called the *global rigidity* property. For inversive distance circle packing and combinatorial Yamabe flow cases with both $\mathbb{E}^2$ and $\mathbb{H}^2$ background geometries (see Figure 4 (c) and (d)) only local rigidity holds. This is caused by the non-convexity of their metric spaces. In practice, non-global rigidity causes many difficulties.

Discrete Ricci flow and entropy energy. In all configurations, the discrete Ricci flow is defined as follows:

$$\frac{du_i(t)}{dt} = (\bar{K}_i - K_i), \tag{9}$$

where $\bar{K}_i$ is the user defined target curvature and K_i is the curvature induced by the current metric. The discrete Ricci flow has exactly the same form as the smooth Ricci flow, which conformally deforms the discrete metric according to the Gaussian curvature.

The discrete Ricci flow can be formulated in the variational setting, namely, it is a negative gradient flow of a special energy form, the so-called *entropy energy*. The energy is given by

$$f(\mathbf{u}) = \int_{\mathbf{u_0}}^{\mathbf{u}} \sum_{i=1}^{n} (\bar{K}_i - K_i)\, du_i, \tag{10}$$

where $\mathbf{u_0}$ is an arbitrary initial metric.

Computing the desired metric with user-defined curvature $\{\bar{K}_i\}$ is equivalent to minimizing the discrete entropy energy. In the case of the tangential circle packing metric with both Euclidean and hyperbolic background geometries, the discrete Ricci energy (see (10)) was first proven to be strictly convex in the seminal work of Colin de Verdiere [11]. It was generalized to the general circle packing metric in [10]. The global minimum uniquely exists, corresponding to the desired metric, which induces the prescribed curvature. The discrete Ricci

flow converges to this global minimum. Although the spherical Ricci energy is not strictly convex, the desired metric $\bar{\mathbf{u}}$ is still a critical point of the energy.

The Hessian matrices for discrete entropy are positive definite for both the Euclidean case (with one normalization constraint $\sum_i u_i = 0$) and the hyperbolic case. The energy can be optimized using Newton's method. The Hessian matrix can be computed using the following formula. For all configurations with Euclidean metric, suppose the distance from the radial circle center to edge $[v_i, v_j]$ is d_{ij} as shown in Figure 5 (right), then

$$\frac{\partial \theta_i}{\partial u_j} = \frac{d_{ij}}{l_{ij}};$$

furthermore

$$\frac{\partial \theta_j}{\partial u_i} = \frac{\partial \theta_i}{\partial u_j}, \qquad \frac{\partial \theta_i}{\partial u_i} = -\frac{\partial \theta_i}{\partial u_j} - \frac{\partial \theta_i}{\partial u_k}.$$

We define the edge weight w_{ij} for edge $[v_i, v_j]$, which is adjacent to $[v_i, v_j, v_k]$ and $[v_j, v_i, v_l]$ as

$$w_{ij} = \frac{d_{ij}^k + d_{ij}^l}{l_{ij}}.$$

The Hessian matrix $H = (h_{ij})$ is given by the discrete Laplace form

$$h_{ij} = \begin{cases} 0, & [v_i, v_j] \notin E, \\ -w_{ij}, & i \neq j, \\ \sum_k w_{ik}, & i = j. \end{cases}$$

With hyperbolic background geometry, the computation of the Hessian matrix is much more complicated. In the following, we give the formula for one face directly, for both circle packing cases:

$$\begin{pmatrix} d\theta_i \\ d\theta_j \\ d\theta_k \end{pmatrix} = \frac{-1}{A} \begin{pmatrix} 1-a^2 & ab-c & ca-b \\ ab-c & 1-b^2 & bc-a \\ ca-b & bc-a & 1-c^2 \end{pmatrix} \begin{pmatrix} \frac{1}{a^2-1} & 0 & 0 \\ 0 & \frac{1}{b^2-1} & 0 \\ 0 & 0 & \frac{1}{c^2-1} \end{pmatrix} \cdot \begin{pmatrix} 0 & ay-z & az-y \\ bx-z & 0 & bz-x \\ cx-y & cy-x & 0 \end{pmatrix} \begin{pmatrix} du_i \\ du_j \\ du_k \end{pmatrix},$$

where $(a, b, c) = (\cosh l_i, \cosh l_j, \cosh l_k)$ and $(x, y, z) = (\cosh \gamma_i, \cosh \gamma_j, \cosh \gamma_k)$, A is double the area of the triangle $A = \sinh l_i \sinh l_j \sin \theta_k$.

For hyperbolic Yamabe flow case,

$$\frac{\partial \theta_i}{\partial u_j} = \frac{\partial \theta_j}{\partial u_i} = \frac{-1}{A} \frac{1+c-a-b}{1+c}$$

and

$$\frac{\partial \theta_i}{\partial u_i} = \frac{-1}{A} \frac{2abc - b^2 - c^2 + ab + ac - b - c}{(1+b)(1+c)}.$$

For tangential and general circle packing cases, with both $\mathbb{R}^2$ and $\mathbb{H}^2$ background geometries, Newton's method leads to the solution efficiently. For the inversive distance circle packing case and the combinatorial Yamabe flow case, with both $\mathbb{R}^2$ and $\mathbb{H}^2$ background geometries, because of the non-convexity of the metric spaces, Newton's method may get stuck at the boundary of the metric spaces; this creates some intrinsic difficulty in practical computation.

Algorithmic details for general combinatorial Ricci flow can be found in [41], inversive distance circle packing metric in [70], and combinatorial Yamabe flow in [72].

3.2. Gu-Yau's method: holomorphic differentials. Gu-Yau's method computes the Holomorphic 1-form group on a metric surface based on Hodge theory. This method is more efficient and stable than the discrete Ricci flow method.

3.2.1. Classical Hodge theory. Suppose the metric surface $(S, \mathbf{g})$ is with isothermal coordinate charts $\{(U_\alpha, \phi_\alpha)\}$. On a local chart (U_α, ϕ_α), the local coordinates are $z_\alpha = u_\alpha + iv_\alpha$. A real differential 1-form τ has the local representation

$$\tau = f_\alpha(u_\alpha, v_\alpha)\, du_\alpha + g_\alpha(u_\alpha, v_\alpha)\, dv_\alpha.$$

The exterior differential operator d acts on τ

$$d\tau = \left(\frac{\partial g_\alpha}{\partial u_\alpha} - \frac{\partial f_\alpha}{\partial v_\alpha} \right) du_\alpha \wedge dv_\alpha.$$

The Hodge star operator $\star$ acts on τ

$$\star\tau = f_\alpha(u_\alpha, v_\alpha)\, dv_\alpha - g_\alpha(u_\alpha, v_\alpha)\, du_\alpha.$$

The *co-differential operator* δ is defined as $\delta = -\star d \star$. If both $d\tau = 0$ and $\delta\tau = 0$, then τ is called a *harmonic 1-form.*

Theorem 3.4 (Hodge [47, Thm. 5.1, p. 280])**.** *Consider the de Rham cohomology group $H^k(S, \mathbb{R})$, each cohomologous class has a unique harmonic form.*

ω is a complex differential form, such that on each local chart with complex coordinates z_α,

$$\omega = f_\alpha(z_\alpha)\, dz_\alpha,$$

where f_α is a holomorphic function,

$$\frac{\partial f_\alpha(z_\alpha)}{\partial \bar{z}_\alpha} = 0,$$

then ω is called a *holomorphic differential 1-form.* Furthermore, ω can be decomposed as two conjugate harmonic 1-forms,

$$\omega = \tau + \sqrt{-1} \star \tau.$$

All the holomorphic 1-forms form a group, our goal is to compute the basis of the group.

3.2.2. Discrete Hodge theory. In the discrete case, we triangulate the surface to a simplicial complex (a triangular mesh), and build chain complexes. The 0, 1 and 2 dimensional simplexes are vertices, edges and faces. A k-simplex, formed by vertices $\{v_0, v_1, \ldots, v_k\}$ in a specific order, is denoted as $[v_0, v_1, \ldots, v_k]$. The k-dimensional chain space is defined as

$$C_k = \left\{ \sum_i z_i \sigma_i,\ z_i \in \mathbb{Z} \right\},$$

where $\{\sigma_i\}$ are all the k-simplexes in the mesh. The boundary operators are linear operators

$$\partial_k \colon C_k \to C_{k-1},$$

$\partial_0 v_i = 0$, $\partial[v_0, v_1] = v_1 - v_0$, $\partial[v_0, v_1, v_2] = [v_0, v_1] + [v_1, v_2] + [v_2, v_0]$. The k-th simplicial homology group is given by

$$H_k(M, \mathbb{Z}) = \operatorname{Ker} \partial_k / \operatorname{Img} \partial_{k+1}.$$

The *co-chain spaces* C^k is defined as

$$C^k = \{\text{linear functionals on } C_k\}.$$

The *discrete exterior differential operator* $d_k \colon C^k \to C^{k+1}$ is a linear operator. Suppose $\sigma \in C_{k+1}$ is a $(k+1)$-chain, $\omega \in C^k$ is a k-cochain, then d_k is defined as

$$(d_k \omega)(\sigma) = \omega(\partial_{k+1} \sigma).$$

The k-th simplicial cohomology group is given by

$$H^k(M, \mathbb{Z}) = \operatorname{Ker} d_k / \operatorname{Img} d_{k+1}.$$

Suppose S is a triangle mesh, its *Poincaré dual* $\tilde{S}$ is its Voronoi diagram. Let $v_i \in S$ be a vertex, then $\tilde{v}_i$ is a 2-cell in $\tilde{S}$,

$$\tilde{v}_i := \{p \in S \colon d(p, v_i) \leq d(p, v_j) \text{ for all } j \neq i\}$$

where d is the metric on the polygonal surface. Let $\sigma \in S$ be an edge, then its dual $\tilde{\sigma}$ is given by

$$\tilde{\sigma} = \bigcap_{v \in \partial\sigma} \tilde{v}.$$

Let $\omega \in C^k$ be a k-form on S, then the *discrete Hodge star operator* is defined as

$$\star \colon C^k(S) \to C^{2-k}(\tilde{S}), \qquad \star\omega(\tilde{\sigma}) = \frac{|\tilde{\sigma}|}{|\sigma|}\, \omega(\sigma),$$

where $|\cdot|$ represents the volume of the simplex σ. The *discrete co-exterior-differential operator* δ is defined as $\delta = - \star d \star$. A *discrete harmonic k-form* $\omega \in C^1$ satisfies $d\omega = 0, \delta\omega = 0$.

Theorem 3.5 (Discrete Hodge)**.** *Suppose S is a polyhedral surface, then each cohomologous class in $H^k(S, \mathbb{R})$ has a unique discrete harmonic k-form.*

3.2.3. Algorithm.

Step 1. Homology basis. We compute a *CW-cell decomposition* of the surface represented as a triangle mesh,

$$S_0 \subset S_1 \subset S_2 = S,$$

where the *k-dimensional skeleton* $S_k = S_{k-1} \cup D_k^1 \cup D_k^2 \cup \cdots \cup D_k^n$, D_k^i are k-dimensional cells (disks), such that the boundaries of these cells are on S_{k-1},

$$\partial D_k^i \subset S_{k-1}.$$

All the loop generators of S_1 $\{\gamma_1, \gamma_2, \ldots, \gamma_{2g}\}$ form a basis for the fundamental group $\pi_1(S)$. These loops also form a basis of the first homology basis $H_1(S, \mathbb{Z})$. Figure 6 shows the homology group generators of a genus two surface.

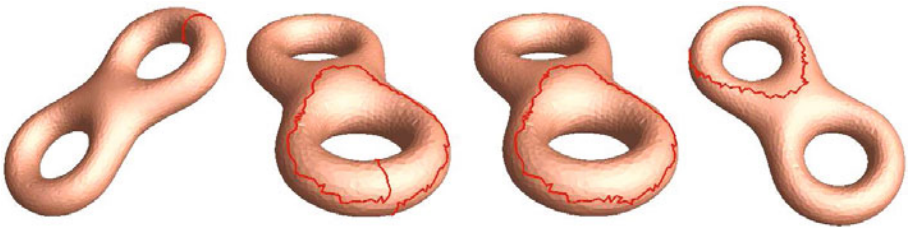

FIGURE 6. Computing homology group basis.

Step 2. Cohomology group basis. Let γ_k be a base loop for $H_1(S, \mathbb{Z})$, then we slice S along γ_k to get an open surface $\tilde{S}_k$, such that the boundary of $\tilde{S}_k$ is given by

$$\partial \tilde{S}_k = \gamma_k^+ - \gamma_k^-,$$

$\gamma_k^+, \gamma_k^{-1}$ are the two boundary loops on $\tilde{S}_k$. Then we construct a function $h_k \colon \tilde{S}_k \to \mathbb{R}$, such that

$$h_k(p) = 1 \quad \text{for all } p \in \gamma_k^+; \qquad h_k(p) = 0 \quad \text{or all } p \in \gamma_k^-;$$

and $h_k(p)$ is random for all interior points on $\tilde{S}_k$. Then dh_k is an exact 1-form on $\tilde{S}_k$. Because of the consistency along the boundaries, dh_k is also a closed 1-form (but not exact) on S, denoted as τ_k. Then the set

$$\{\tau_1, \tau_2, \ldots, \tau_{2g}\}$$

forms a basis for the first cohomology group $H^1(S, \mathbb{R})$.

Step 3. Harmonic 1-form basis. According to the Hodge theory, for each closed 1-form τ_k, there exists a 0-form $g_k \colon S \to \mathbb{R}$, such that $\tau_k + dg_k$ is a harmonic 1-form. The 0-form g_k can be obtained by solving $\delta(\tau_k + dg_k) = 0$, where δ is the co-differential operator. We denote the harmonic 1-form as $\omega_k = \tau_k + dg_k$. Then the set

$$\{\omega_1, \omega_2, \ldots, \omega_{2g}\}$$

forms a basis for the cohomology group $H^1(S, \mathbb{R})$.

By direct computation, the *discrete co-exterior differential operator* $\delta \colon C^1 \to C^0$ has the formula

$$\delta(\omega)(v_i) = \sum_{[v_i, v_j] \in \Sigma} w_{ij}(\omega[v_j, v_i]),$$

where w_{ij} is the cotangent edge weight 14. Figure 7 shows the harmonic 1-form group generators of a genus two surface.

FIGURE 7. Computing harmonic 1-form group basis.

Step 4. Holomorphic 1-form basis. A holomorphic 1-form can be constructed by a harmonic 1-form and its conjugate $\omega_k + i \star \omega_k$, where $\star$ is the Hodge star operator. The conjugate form of a harmonic 1-form is still a harmonic 1-form, in the space spanned by $\{\omega_i\}$, and thus can be expressed using linear combinations of the ω_i's. Therefore,

$$\star\omega_k = \sum_{i=1}^{2g} c_{ki}\omega_i,$$

where c_{ki}'s are unknown real numbers. By solving the following linear system

$$\int_S \omega_j \wedge \star\omega_k = \sum_{i=1}^{2g} c_{ki} \int_S \omega_j \wedge \omega_i, \qquad j = 1, 2, \ldots, 2g, \tag{11}$$

we can find all the unknowns and get the conjugate form. Then the set

$$\{\omega_1 + i \star \omega_1, \omega_2 + i \star \omega_2, \ldots, \omega_{2g} + i \star \omega_{2g}\}$$

forms a basis for the holomorphic 1-form group of the surface.

The *discrete wedge operator* $\wedge\colon C^1 \times C^1 \to C^2$ is defined as follows. Given $[v_i, v_j, v_k] \in \Sigma$, $\omega_1, \omega_2 \in C^1$ are discrete closed 1-forms, then

$$\omega_1 \wedge \omega_2([v_i, v_j, v_k]) = \frac{1}{2} \begin{vmatrix} \omega_1([v_i, v_j]) & \omega_2([v_i, v_j]) \\ \omega_1([v_j, v_k]) & \omega_2([v_j, v_k]) \end{vmatrix}.$$

Let ω, τ be two discrete harmonic 1-forms, where locally $\omega = c_1 dx + c_2 dy$ and $\tau = d_1 dx + d_2 dy$, then locally

$$\omega \wedge \star\tau = \begin{vmatrix} c_1 & c_2 \\ d_1 & d_2 \end{vmatrix} dx \wedge dy.$$

Figure 8 shows the holomorphic 1-form group basis for the genus two surface.

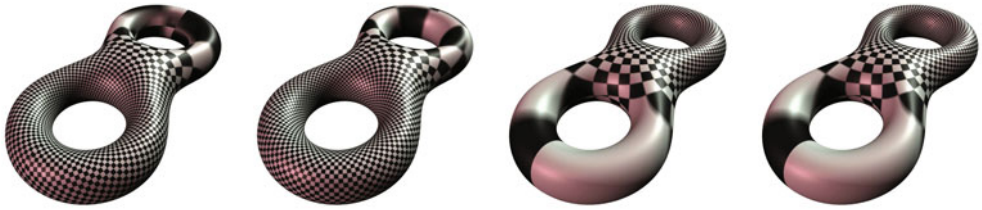

FIGURE 8. Computing holomorphic 1-form group basis.

3.3. Non-linear heat flow. The non-linear heat flow method can be applied to compute conformal maps between genus zero closed surfaces.

3.3.1. Classical surface harmonic maps. For the 2-sphere in the standard metric, we have,

Theorem 3.6 (Schoen and Yau [59, Cor. p. 12])**.** *Harmonic maps between genus zero closed metric surfaces are conformal maps.*

In order to compute a conformal map from a topological sphere S to the unit sphere $\mathbb{S}^2$, $\phi\colon S \to \mathbb{S}^2$, we only need to compute a harmonic map between them. Harmonic maps can be computed using the *heat flow method*,

$$\frac{\partial \phi(p,t)}{\partial t} = -\Delta_p \phi(p,t).$$

The initial map $\phi(p, 0)$ can be set as the *Gauss map*, where $p \in S$ is a point on the surface and $\mathbf{n}(p) \in \mathbb{S}^2$ is the normal at p. The Gauss map is $\phi(p, 0) = \mathbf{n}(p)$. Because $\mathbb{S}^2$ is embedded in $\mathbb{R}^3$, we treat ϕ as a vector valued function $\phi = (\phi_1, \phi_2, \phi_3)$, where each ϕ_k is a function. Then its Laplacian is given by

$$\Delta_p \phi(p,t) = (\Delta_p \phi_1(p,t), \Delta_p \phi_2(p,t), \Delta_p \phi_3(p,t)).$$

Then we project the Laplacian to the tangent spaces of $\phi(p)$. The normal component of the Laplacian is given by

$$\Delta_p^{\perp}\phi(p,t) = \langle \Delta_p \phi(p,t), \phi(p,t)\rangle \phi(p,t),$$

where $\langle\cdot,\cdot\rangle$ is the inner product in $\mathbb{R}^3$. The tangential component of the Laplacian is given by

$$\Delta_p^{\parallel}\phi(p,t) = \Delta_p\phi(p,t) - \Delta_p^{\perp}\phi(p,t).$$

Definition 3.7 (Non-linear heat flow)**.** Non-linear heat flow is defined as

$$\frac{\partial \phi(p,t)}{\partial t} = -\Delta_p^{\parallel}\phi(p,t).$$

The *stereographic projection* maps the unit sphere to the whole complex plane, $\tau\colon \mathbb{S}^2 \to \mathbb{C}$,

$$\tau(x,y,z) = \left(\frac{x}{1-z}, \frac{y}{1-z}\right).$$

Let ρ be a *Möbius transformation*,

$$\rho(z) = \frac{az+b}{cz+d}, \qquad a,b,c,d \in \mathbb{C},\ ad-bc=1. \tag{12}$$

$\tau^{-1}\circ\rho\circ\tau\colon \mathbb{S}^2 \to \mathbb{S}^2$ is a conformal mapping of the unit sphere. All such mappings form a 6 dimensional group, the so-called *spherical Möbius transformation group.*

Because the conformal maps are not unique, differing by a Möbius transformation on the sphere, a special normalization condition needs to be added during the flow. The following is a common condition,

$$\int_S \phi(p)\, ds = 0. \tag{13}$$

For genus zero closed surfaces, harmonic maps are conformal.

3.3.2. Discrete surface harmonic maps. On a discrete surface Σ, the functions are approximated by piecewise linear functions. Suppose $[v_i, v_j, v_k]$ is a face, for any point $p \in [v_i, v_j, v_k]$, the barycentric coordinates of p are

$$p = \alpha v_i + \beta v_j + \gamma v_k, \qquad 0 \le \alpha, \beta, \gamma \le 1,\ \alpha+\beta+\gamma = 1,$$

then $f(p) = \alpha f(v_i) + \beta f(v_j) + \gamma f(v_k)$. By the Finite Element Method [53], the *discrete harmonic energy* of f has the representation

$$E(f) = \frac{1}{2}\sum_{[v_i,v_j]\in\Sigma} w_{ij}(f(v_i) - f(v_j))^2,$$

where w_{ij} is the *edge weight*

$$w_{ij} = \cot\theta_{ij}^k + \cot\theta_{ij}^l, \tag{14}$$

θ_{ij}^k is the corner angle on face $[v_i, v_j, v_k]$ at the vertex v_k, and θ_{ij}^l is the corner angle on face $[v_i, v_j, v_l]$ at the vertex v_l. If $[v_i, v_j]$ is only adjacent to one face $[v_i, v_j, v_k]$,

then the term $\cot\theta_{ij}^l$ should be omitted. Similarly, the discrete *Laplace-Beltrami operator* is given by

$$\Delta f(v_i) = \sum_{[v_i,v_j]\in\Sigma} w_{ij}(f(v_i) - f(v_j)).$$

We can compute the Gauss map first, then diffuse the Gauss map to a harmonic map with the normalization condition (13). Algorithmic details for discrete spherical harmonic maps can be found in [31].

4. Conformal modulus and conformal mapping

In this section, we apply the discrete surface Ricci flow and holomorphic differential methods to compute conformal mappings of surfaces with various topologies.

4.1. Topological quadrilateral. Suppose S is a surface of genus zero with a single boundary, and four marked boundary points $\{p_1, p_2, p_3, p_4\}$ sorted counterclockwise. Then S is called a topological quadrilateral, and denoted as $Q(p1, p2, p3, p4)$. There exists a unique conformal map $\phi\colon S \to \mathbb{C}$, such that ϕ maps Q to a rectangle, $\phi(p_1) = 0$, $\phi(p_2) = 1$.

Holomorphic differential method. Assume the boundary of Q consists of four segments $\partial Q = \gamma_1 + \gamma_2 + \gamma_3 + \gamma_4$, such that

$$\partial\gamma_1 = p_2 - p_1, \qquad \partial\gamma_2 = p_3 - p_2, \qquad \partial\gamma_3 = p_4 - p_3, \qquad \gamma_4 = p_1 - p_4.$$

We compute two harmonic functions $f_1, f_2 \to \mathbb{R}$, such that

$$\begin{cases} \Delta f_1 = 0 \\ f_1|_{\gamma_1} = 0 \\ f_1|_{\gamma_3} = 1 \\ \dfrac{\partial f_1}{\partial n}|_{\gamma_2\cup\gamma_4} = 0 \end{cases} \qquad \begin{cases} \Delta f_2 = 0 \\ f_2|_{\gamma_2} = 0 \\ f_2|_{\gamma_4} = 1 \\ \dfrac{\partial f_2}{\partial n}|_{\gamma_1\cup\gamma_3} = 0 \end{cases}$$

with the Laplace-Beltrami operator $\Delta = d\delta + \delta d$. On a surface, $\Delta f = 0$ is equivalent to $\delta df = 0$. The df_1 and df_2 are two exact harmonic 1-forms. We need to find a scalar λ, such that $\star df_1 = \lambda df_2$, this can be achieved by solving the following equation,

$$\int_S df_1 \wedge \star df_1 = \lambda \int_S df_1 \wedge df_2.$$

The geometric interpretation of λ is the conformal modulus of the quadrilateral. Then the desired holomorphic 1-form $\omega = df_1 + i\lambda df_2$. The conformal mapping is given by

$$\phi(p) = \int_q^p \omega,$$

where q is the base point and the path from q to p is arbitrarily chosen. Figure 9 shows the conformal mapping of a topological quadrilateral to the planar rectangle.

(a) Input surface (b) Conformally mapped to a rectangle (c) Checkerboard texture mapping

FIGURE 9. Conformal module for a topological quadrilateral. The face surface with four boundary corners (a) is conformally mapped to a planar rectangle (b). A checkerboard texture is placed on the rectangle and pulled back to the face surface (c), all the right angles of checkers are well preserved.

Ricci flow method. We can set the target Gaussian curvature to be zero everywhere, except at the four corners $\{p_1, p_2, p_3, p_4\}$, where the target curvatures are set to be $\pi/2$. Then we run Euclidean Ricci flow, which gives us a flat metric on the surface. By isometrically embedding the surface onto the plane, we map the surface onto a planar rectangle.

4.2. Topological annulus. Suppose S is a topological annulus with a Riemannian metric $\mathbf{g}$ and the boundary of S are two loops $\partial S = \gamma_1 - \gamma_2$, then there exists a conformal mapping $\phi\colon S \to \mathbb{C}$, which maps S to the canonical annulus, $\phi(\gamma_1)$ is the unit circle and $\phi(\gamma_2)$ is another concentric circle with radius γ. The mapping ϕ is unique up to a planar rotation.

Holomorphic 1-form method. The holomorphic 1-form group is one dimensional. We compute the generator ω, such that $\operatorname{Img}\omega(dr) = 0$, where dr is any tangent vector along the boundary, and $\int_{\gamma_1}\omega = 1$. Let p be a base point on the surface, for any other point q, define

$$\phi(q) = \exp\left(2\pi i \int_p^q \omega\right).$$

ϕ is the desired conformal mapping, as shown in Figure 10.

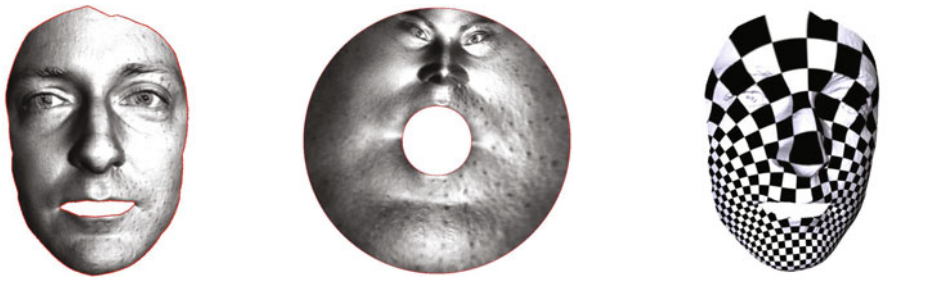

(a) Input surface (b) Conformally mapped to an annulus (c) Checkerboard texture mapping

FIGURE 10. Conformal module for a topological annulus. The face surface (a) is conformally mapped to a planar annulus (b). A checkerboard texture is placed on the annulus and pulled back to the face surface (c), all the right angles of checkers are well preserved.

Ricci flow method. We can set the target Gaussian curvature to be zero everywhere, including the boundary vertices, and run Euclidean discrete surface Ricci flow, then we obtain a flat metric. We find a curve γ connecting γ_1 and γ_2, such that γ is a straight line segment under the flat metric and orthogonal to the two boundaries. We slice the surface along γ to get $\tilde{S}$, and γ becomes two boundary segments γ^+ and γ^-. We then isometrically embed $\tilde{S}$ onto the plane. After a planar rigid motion, and a normalization, $\tilde{S}$ is a rectangle with unit height, and γ^- is on the real axis, γ_1 is on the imaginary axis. Then we use the exponential map $z \mapsto \exp(2\pi i z)$ to map $\tilde{S}$ to the canonical planar annulus.

4.3. Topological disk. Suppose S is a topological disk with a Riemannian metric, then it can be conformally mapped to the unit planar disk. Two such mappings differ by a Möbius transformation

$$z \mapsto e^{i\theta} \frac{z - z_0}{1 - \bar{z}_0 z}, \tag{15}$$

as shown in Figure 11.

FIGURE 11. Riemann mapping for a topological disk. Two such mappings differ by a Möbius transformation.

The computation is straight forward. We punch a small hole at the point z_0 to make the surface a topological annulus and map the annulus onto the canonical planar annulus using the method in the last subsection. When the size of the punched holes shrink to a point, the mappings obtained converge to the real Riemann mapping.

4.4. Multiply connected domain. Suppose S is a surface of genus zero with multiple boundaries, then S is called a multiply connected domain. Suppose S is a multiply connected domain with a Riemannian metric $\mathbf{g}$, then there exists a conformal mapping $\phi\colon S \to \mathbb{C}$, which maps S to the unit disk with circular holes. Such conformal mappings are unique up to Möbius transformations.

Let S be the multiply connected domain, then its boundary consists of n connected components,

$$\partial S = \gamma_0 - \gamma_1 - \gamma_2 \ldots - \gamma_n,$$

where γ_0 is the exterior boundary and $\{\gamma_k, k > 0\}$ are sorted by their total lengths. There are two methods to compute the conformal modulus and the conformal mapping.

Ricci flow method. We set the target curvature in the following way:

(i) For all interior vertices $v_i \notin \partial S$, $\bar{K}(v_i)$ is zero.
(ii) For all vertices on γ_0 or γ_1, $\bar{K}(v_i)$ is zero.
(iii) Let $v_i \in \gamma_k, k \neq 0, 1$, suppose the total length under the current metric is $|\gamma_k|$, the two boundary edges attaching to v_i are e_i and e_{i+1}, then set

$$\bar{K}(v_i) = -\pi \frac{|e_i| + |e_{i+1}|}{|\gamma_k|}.$$

Note that in the curvature flow, the edge lengths $|e_i|, |e_{i+1}|, |\gamma_k|$ are changing. Therefore, the $\bar{K}(v_i)$ need to be updated accordingly.

By running discrete curvature flow with time variant target curvature, the procedure will converge, and a unique flat metric will be obtained. Then we find a shortest path τ connecting γ_0 and γ_1, and slice S along τ to get a surface $\tilde{S}$. The flat metric will flatten $\tilde{S}$ onto a planar parallelogram with circular holes. Then we use an exponential map to map the parallelogram to a disk with circular holes.

Generalized Koebe's method. The algorithm is based on using the holomorphic 1-form to compute the conformal mapping of a topological annulus.

(i) Fill all boundary γ_k's with topological disks D_k's such that $\partial D_k = \gamma_k$, $k = 0, 1, 2, \ldots, n$. The resulting surface is a topological sphere $\tilde{S}$ with $\tilde{S} = S \cup D_0 \cup D_1 \cup \cdots \cup D_n$.
(ii) Remove two disks D_i and D_j from $\tilde{S}$, denote the topological annulus as $\tilde{S}_{ij} = \tilde{S}/\{D_i \cup D_j\}$.

(iii) Map the annulus $\tilde{S}_{ij}$ to a canonical planar annulus, denote the image of ϕ as $\tilde{S}_{ij}$.

(iv) Choose another two disks D_k and D_l, further remove them from $\tilde{S}_{ij}$, denoted the three holed annulus as $\tilde{S}_{ijkl} = \tilde{S}_{ij}/\{D_k \cup D_l\}$.

(v) Compute a small circle (c_k, r_k) completely contained in γ_k, reflect $\tilde{S}_{ijkl}$ with respect to the small circle

$$z \mapsto \frac{{r_k}^2}{|z - c_k|^2}(z - c_k) + c_k,$$

this maps γ_i, γ_j to be interior circles, and γ_k to be the exterior boundary.

(vi) Fill circular holes bounded by γ_i and γ_j by circular disks $\tilde{D}_i$ and $\tilde{D}_j$ such that $\partial\tilde{D}_i = \gamma_i$, $\partial\tilde{D}_j = \gamma_j$, $\tilde{S}_{kl} = \tilde{S}_{ijkl} \cup \tilde{D}_i \cup \tilde{D}_j$.

(vii) Repeat step 3 through 6, until all the holes are circular enough.

The convergence rate is governed by the following theorem. Suppose the surface has n boundary components. At each step, we fill $n-2$ holes and map the surface to an annulus, the remaining 2 boundary components are mapped to the inner and outer circles of the annulus.

Theorem 4.1 (Generalized Koebe [77, Thm. 1.2])**.** *Given a genus zero surface with n boundaries, there exist constants $C_1 > 0$, $0 < C_2 < 1$, for step k, such that $f_k(\infty) = \infty$ and $f_k(z) = z + \mathcal{O}(z^{-1})$ near the ∞ point, for all $z \in \mathbb{C}$,*

$$|f_k \circ f^{-1}(z) - z| < C_1 C_2^{2[k/n]},$$

where f is the limit conformal mapping and $[k/n]$ denotes the greatest integer not exceeding k/n.

Figure 12 shows the canonical conformal mapping of a multiply connected domain, which is a region of a 3D human face surface, obtained by structured light scanning [32].

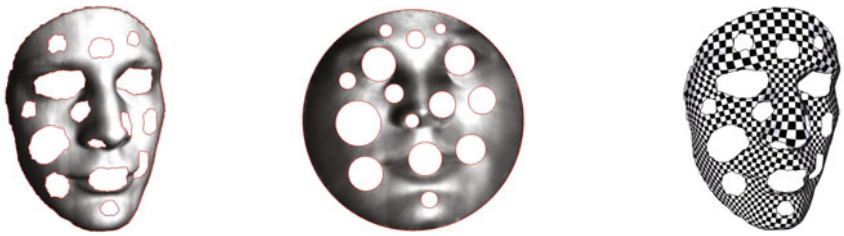

(a) Input surface (b) Conformally mapped to a circle domain (c) Checkerboard texture mapping

FIGURE 12. Conformal module for a topological multiply connected domain. The face surface (a) is conformally mapped to a planar circle domain (b). A checkerboard texture is placed on the circle domain and pulled back to the face surface (c), all the right angles of checkers are well preserved.

Slit map. All multiply connected domains can be conformally mapped to canonical planar domains, which are annuli with concentric circular slits or rectangles with horizontal slits [71].

Suppose the boundary of S is a set of loops $\partial S = \{\gamma_0, \gamma_1, \ldots, \gamma_n\}$, where γ_0 is the exterior boundary. Then a set of basis of holomorphic 1-forms can be found, $\omega_1, \omega_2, \ldots, \omega_n$, such that the integration of ω_i along γ_j equals to δ_{ij}, where δ_{ij} is the Kronecker symbol. Special holomorphic 1-forms can be found, such that

$$\operatorname{Im}\left(\int_{\gamma_i} \omega\right) = \begin{cases} 2\pi, & i = 0, \\ -2\pi, & i = 1, \\ 0, & \text{otherwise.} \end{cases} \tag{16}$$

Then if we choose a base point p_0 on the surface, for any point p, we choose an arbitrary path γ on the surface and define a complex function

$$\phi(p) = \exp\left(\int_{\gamma} \omega\right),$$

which maps the surface to an annulus. γ_0 is mapped to the outer boundary, γ_1 to the inner boundary, and all other boundaries are mapped to the concentric circular slits. Then the (complex) logarithm of ϕ maps the surface periodically to a rectangle, with all the circular slits mapped to horizontal slits. We call ϕ a *circular slit map* and $\log \phi$ a *horizontal slit map*.

The algorithm for computing a slit map is straightforward.

(i) Compute a set of holomorphic 1-form bases of the surface, $\{\omega_i\}$.
(ii) Compute a holomorphic 1-form represented as the linear combination of the basis $\omega = \sum \lambda_i \omega_i$, such that (16) holds.

Figure 13 shows the circular and horizontal slit maps for a multiply connected annulus with 3 holes.

FIGURE 13. Slit map for a multiply connected domain.

Crowdy and Marshall [16] introduced a constructive method to compute conformal mappings between canonical multiply connected domains, which is based

on Green's functions and harmonic measures in potential theory. Our holomorphic differential method is similar to their construction, because the holomorphic 1-form satisfying (16) is closely related to harmonic measure.

4.5. Genus zero closed surface. The genus zero closed surface can be conformally mapped to a unit sphere. The mapping is not unique, two such conformal mappings differ by a spherical Möbius transformation, as shown in Figure 14.

FIGURE 14. Genus zero closed surface.

Harmonic map method. Given a genus zero closed surface S, first we compute the Gauss map $\phi\colon S \to \mathbb{S}^2$, then use the non-linear heat diffusion method to optimize the harmonic energy with a normalization condition, such that the mass center of the image surface is at the origin. Figure 14 shows a conformal mapping from a brain cortical surface to the unit sphere.

Holomorphic 1-form method. We first remove one triangle and make the genus zero surface become a topological disk. Then we conformally map it to a planar triangle by the holomorphic 1-form method and then obtain the unit sphere by the *inverse stereographic projection*,

$$(x, y, z) = \left(\frac{2u}{1+u^2+v^2}, \frac{2v}{1+u^2+v^2}, \frac{-1+u^2+v^2}{1+u^2+v^2} \right), \qquad (u, v) \in \mathbb{C}.$$

Then we move the mass center of the image to the origin with a spherical Möbius transformation. We can also use a curvature flow map to map the topological disk to the plane.

Inversely, for a topological disk, we can convert it to a genus zero closed symmetric surface by *doubling*, and then map the doubled surface to the unit sphere. The hemispherical conformal mapping of the original surface is obtained. As shown in Figure 15, the conformal mapping preserves the intrinsic symmetry of the doubled surface. The image of the mapping and the area distortion factor on the image are both symmetric.

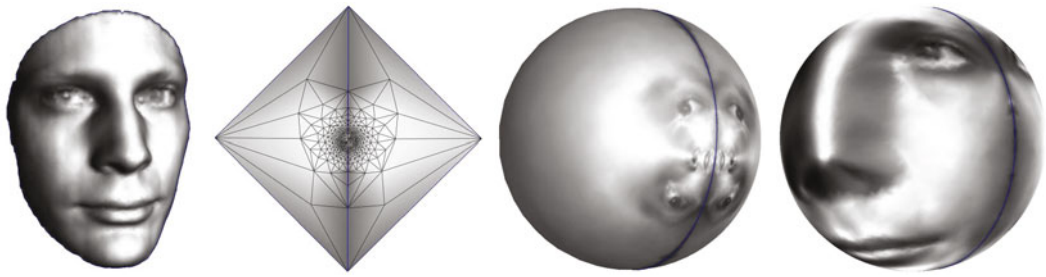

FIGURE 15. Spherical map for a topological disk by doubling.

4.6. Genus one closed surface.

Holomorphic 1-form method. First we compute a basis for the fundamental group $\pi_1(S)$, $\{\gamma_1, \gamma_2\}$. Then we compute the holomorophic 1-form basis ω_1, ω_2, such that

$$\int_{\gamma_i} \omega_j = \delta_{ij}.$$

Then we slice the surface along γ_1, γ_2 to get a fundamental domain $\tilde{S}$. The conformal mapping $\phi\colon \tilde{S} \to \mathbb{C}$ is given by

$$\phi(p) = \int_q^p \omega_1,$$

where q is the base point; the path from q to p in $\tilde{S}$ can be arbitrarily chosen. Suppose $a + ib = \int_{\gamma_2} \omega_1$, then $a + ib$ is the conformal modulus of the torus. The deck transformation group generators are

$$T_1(z) = z + 1, \qquad T_2(z) = z + a + ib.$$

By using all deck transformations to translate $\phi(\tilde{S})$, we can conformally map the universal covering space of S onto the whole complex plane $\mathbb{C}$; the fundamental domain of the lattice generated by $\{T_1, T_2\}$ is a parallelogram.

Curvature flow method. We can set the target curvature to be zero everywhere, and run Ricci flow to compute a flat metric conformal to the original metric. Then we can isometrically flatten the fundamental domain $\tilde{S}$ onto the complex plane, denoting the mapping as ϕ. The deck transformation generators are given by the translations $\{T_1, T_2\}$. T_1 maps $\phi(\gamma_1^+)$ to $\phi(\gamma_1^-)$ and T_2 maps $\phi(\gamma_2^+)$ to $\phi(\gamma_2^-)$.

Figure 16 shows the computational result for a genus one closed surface.

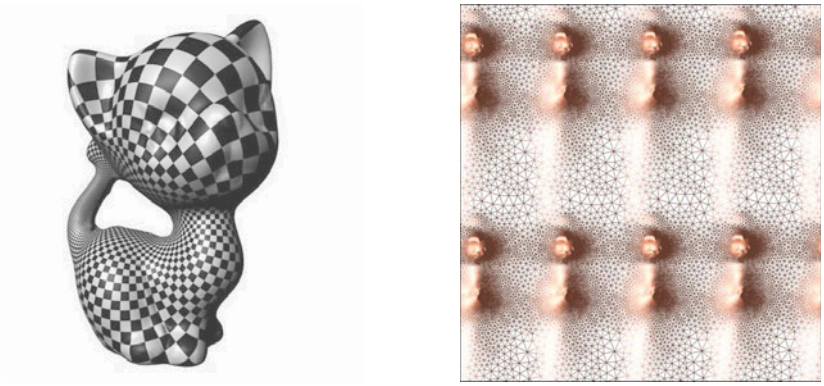

FIGURE 16. Genus one closed surface.

4.7. Genus one surface with boundaries. We use the Ricci flow method to compute the canonical conformal mapping and the conformal modulus. Suppose the boundary of the surface has n loops, $\partial S = \gamma_1 + \gamma_2 + \cdots + \gamma_n$. We set the target curvature in the following way:

(i) For all interior vertices $v_i \notin \partial S$, $\bar{K}(v_i)$ is zero.
(ii) Let $v_i \in \gamma_k$, suppose the total length under the current metric is $|\gamma_k|$, the two boundary edges attaching to v_i are e_i and e_{i+1}, then set

$$\bar{K}(v_i) = -\pi \frac{|e_i| + |e_{i+1}|}{|\gamma_k|}.$$

Note that during the curvature flow, the edge lengths $|e_i|, |e_{i+1}|, |\gamma_k|$ are changing. Therefore, the $\bar{K}(v_i)$ are updated accordingly.

By running discrete curvature flow with time variant target curvature, the procedure will converge, and a unique flat metric will be obtained. Then we compute the homology group basis $\{\gamma_1, \gamma_2\}$ and slice the surface along the base loops to get a fundamental domain. By isometric embedding $\tilde{S}$ with the new metric, we get the conformal mapping $\phi\colon \tilde{S} \to \mathbb{C}$. Similarly, we compute the generators of the deck transformation group $\{T_1, T_2\}$, T_1 maps $\phi(\gamma_1^+)$ to $\phi(\gamma_1^-)$, T_2 maps $\phi(\gamma_2^+)$ to $\phi(\gamma_2^-)$. Then we can use the deck transformation to map the whole universal covering space of S onto the complex plane with circular holes.

Figure 17 shows the computational result for a genus one surface with three boundaries, the famous Costa's minimal surface [12].

4.8. High genus surface. For a high genus closed surface, we use hyperbolic Ricci flow to compute the hyperbolic metric by setting the target curvature to be zero everywhere. Then we compute a canonical homology group basis $\{a_1, b_1, a_2, b_2, \ldots, a_g, b_g\}$. Then we slice the surface along the base loops to get a fundamental domain $\tilde{S}$, the boundary of $\tilde{S}$ is $a_1 b_1 a_1^{-1} b_1^{-1} \cdots a_g b_g a_g^{-1} b_g^{-1}$, then isometrically flatten $\tilde{S}$ to the Poincaré disk using the hyperbolic metric.

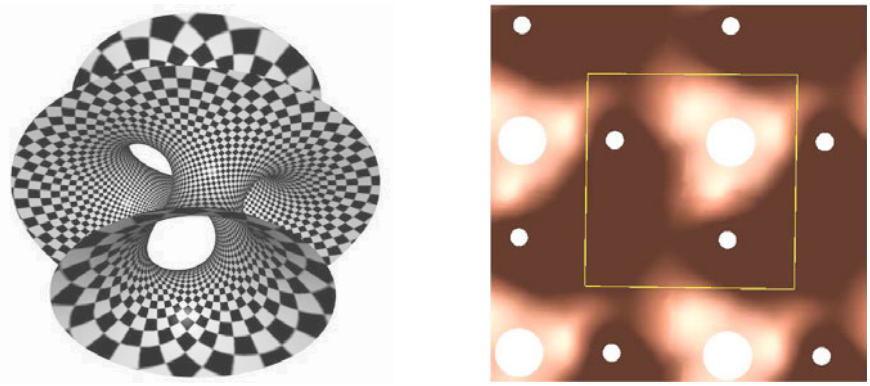

FIGURE 17. Genus one surface with boundaries, Costa's minimal surface [12]

.

The Poincaré disk is the interior of the unit disk $\mathbb{D} = \{z \in \mathbb{C} : |z| < 1\}$ on the complex plane, with hyperbolic metric

$$ds^2 = \frac{dzd\bar{z}}{(1 - z\bar{z})^2},$$

therefore, the Poincaré disk is a conformal model for the hyperbolic space $\mathbb{H}^2$. The hyperbolic lines through p and q are circular arcs passing through p and q, which are orthogonal to the unit circle. The hyperbolic circle (c, r) on the Poincaré disk is identical to the Euclidean circle (C, R),

$$C = \frac{1 - t^2}{1 - t^2 c\bar{c}}c, \qquad R = \sqrt{C\bar{C} - \frac{c\bar{c} - t^2}{1 - t^2 c\bar{c}}}, \qquad t = \tanh\frac{r}{2}.$$

The angles in a hyperbolic triangle can be computed from the edge lengths using the hyperbolic cosine law. Therefore, by using Euclidean geometry we can accomplish all hyperbolic compass and straightedge constructions in the Poincaré disk. We can flatten triangle by triangle and isometrically embed the whole fundamental domain $\tilde{S}$ onto the Poincaré disk. We denote the conformal mapping as $\phi : \tilde{S} \to \mathbb{D}$.

We can then compute the deck transformation group generators. In this case, the deck transformation group is called the *Fuchsian group*. All the Fuchsian transformations are hyperbolic rigid motions, which are Möbius transformations with the form of (15). The Möbius transformation α_k maps the boundary segment $\phi(b_k^{-1})$ to $\phi(b_k)$, the β_k maps $\phi(a_k)$ to $\phi(a_k^{-1})$. Then

$$\{\alpha_1, \beta_1, \alpha_2, \beta_2, \ldots, \alpha_g, \beta_g\}$$

forms a basis set of the Fuchsian group generators.

For high genus surfaces with boundaries, the conformal mapping which maps them to hyperbolic circular domains can be computed in a similar way. According

to Theorem 1.3, the surface can be conformally mapped to the Poincaré disk, such that the boundaries are mapped to hyperbolic circles. By applying hyperbolic Ricci flow with the constraint that the holonomy along each boundary loop is trivial, the hyperbolic metric can be obtained directly.

Figure 18 shows the isometric embedding of finite portions of the universal covering spaces of two high genus surfaces on the Poincaré disk with their uniformization hyperbolic metrics. The algorithmic details can be found in [41].

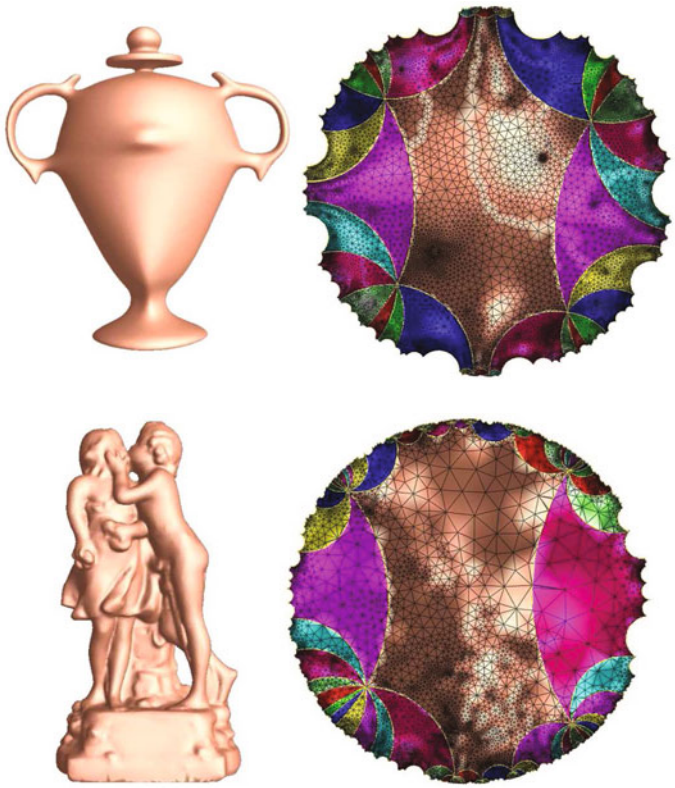

FIGURE 18. Uniformization for high genus surfaces.

5. Applications

Computational conformal geometry has been broadly applied in many engineering fields. In the following, we briefly introduce some of our recent projects, which are the most direct applications of computational conformal geometry in the computer science field.

5.1. Graphics. Conformal geometric methods have broad applications in computer graphics. Isothermal coordinates are natural for global surface parameterization purposes [29]. Because conformal mappings don't distort local shapes, it

is desirable for texture mapping. Figure 19 shows one example of using holomorphic 1-forms for texture mapping.

Special flat metrics are valuable for designing vector fields on surfaces, which plays an important role for non-photorealistic rendering and special art form design. Figure 20 shows the examples for vector fields design on surfaces using the curvature flow method [46].

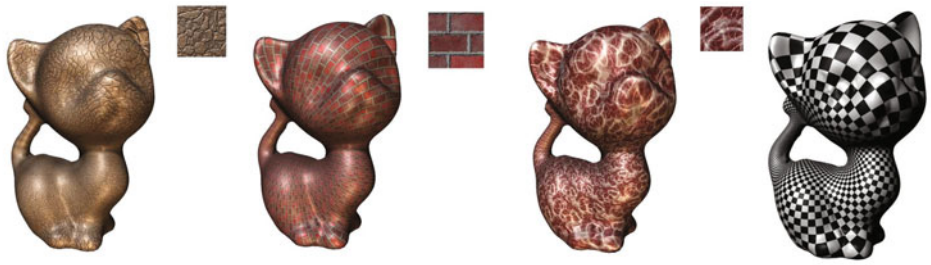

FIGURE 19. Global conformal surface parameterization using holomorphic 1-forms.

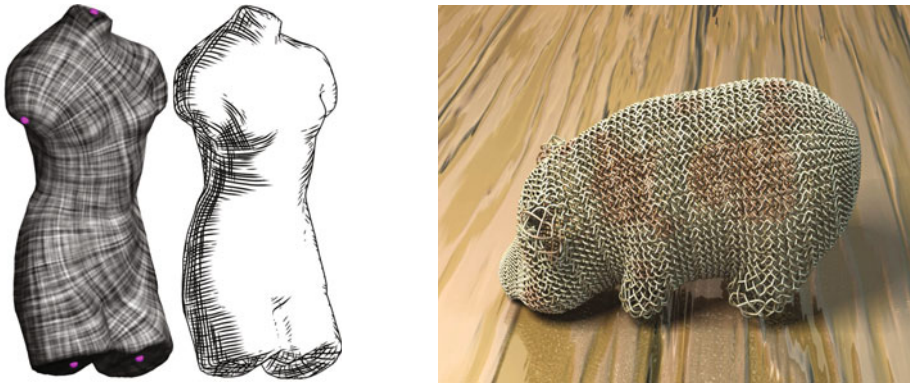

FIGURE 20. Vector field design using special flat metrics.

5.2. Geometric modeling. One of the most fundamental problems in geometric modeling is to systematically generalize conventional spline schemes from Euclidean domains to manifold domains. This relates to the general geometric structures on the surface.

Definition 5.1 ((G, X) structure)**.** Suppose X is a topological space, G is a transformation group of X. Let M be a manifold with an atlas $\mathbb{A}$, if all the coordinate charts (U_α, ϕ_α) are defined on the space X, $\phi_\alpha \colon U_\alpha \to X$; and all chart transition functions $\phi_{\alpha\beta}$ are in group G, then the atlas is a (G, X) atlas. The maximal (G, X) atlas is a (G, X) structure.

For example, suppose the manifold is a surface. If X is the affine plane A, G is the affine transformation group $Aff(A)$, then the (G, X) structure is the affine structure. Similarly, if X is the hyperbolic plane $\mathbb{H}^2$, and G is the hyperbolic isometric transformation (Möbius transformation), then (G, X) is a hyperbolic structure; if X is the real projective plane $\mathbb{RP}^2$, G is the real projective transformation group $PGL(2, R)$, then the (G, X) structure is a real projective structure of the surface. Real projective structure can be constructed from the hyperbolic structure.

Conventional spline schemes are constructed based on affine invariance. If the manifold has an affine structure, then affine geometry can be defined on the manifold and conventional splines can be directly defined on the manifold. Due to the topological obstruction, general manifolds don't have affine structures, but by removing several singularities, general surfaces can admit affine structures. Details can be found in [28].

Affine structures can be explicitly constructed using conformal geometric methods. For example, we can concentrate all the curvatures at the prescribed singularity positions, and set the target curvatures to be zeros everywhere else. Then we use curvature flow to compute a flat metric with cone singularities from the prescribed curvature. The flat metric induces an atlas on the punctured surface (with singularities removed), such that all the transition functions are rigid motions on the plane. Another approach is to use holomorphic 1-forms; a holomorphic 1-form induces a flat metric with cone singularities at the zeros, where the curvatures are $-2k\pi$. Figure 21 shows the manifold splines constructed using the curvature flow method.

FIGURE 21. Manifold splines with extraordinary points (the centers of the yellow regions).

Compared to other methods for constructing domains with prescribed singularity positions, such as the one based on trivial connection [14], the major advantage of this one is that it gives global conformal parameterizations of the spline surface, namely, the isothermal coordinates. Differential operators, such as gradient and Laplace-Beltrami operators, have the simplest form under isothermal coordinates, which greatly simplifies the downstream physical simulation tasks based on the splines.

5.3. Medical imaging. Conformal geometry has been applied for many fields in medical imaging. For example, in the field of brain imaging, it is crucial to register different brain cortex surfaces. Because brain surfaces are highly convoluted, and different people have different anatomic structures, it is quite challenging to find a good matching between cortex surfaces. Figure 14 illustrates one solution [31] by mapping brains to the unit sphere in a canonical way. Then by finding an automorphism of the sphere, the registration between surfaces can be easily established.

In virtual colonoscopy [39], the colon surface is reconstructed from CT images. By using conformal geometric methods, one can flatten the whole colon surface onto a planar rectangle. Then polyps and other abnormalities can be found efficiently on the planar image. Figure 22 shows an example for virtual colon flattening based on conformal mapping.

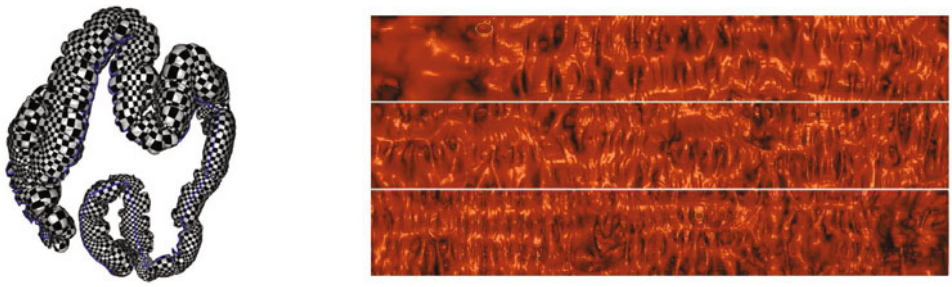

FIGURE 22. Colon conformal flattening.

5.4. Vision. Surface matching is a fundamental problem in computer vision. We focuses on multiply connected surfaces, such as a human face surface, where there are holes for the eyes and mouth. If the surfaces are isometric, then their conformal moduli should match and they can be conformally flattened to the same canonical circle domain. This is the basis for a recognition algorithm. The main framework of surface matching can be formulated as follows:

Suppose S_1, S_2 are two given surfaces, $f\colon S_1 \to S_2$ is the desired matching. We compute $\phi_i\colon S_i \to D_i$ which maps S_i conformally onto the canonical domain D_i. We construct a diffeomorphism map $\bar{f}\colon D_1 \to D_2$, which incorporates the feature

constraints. The final map ϕ is induced by $f = \phi_2 \circ \bar{f} \circ \phi_1^{-1}$. Figure 23 shows one example of surface matching among a human face with different expressions. The human face surfaces are shown on the left,the matching results using consistent texture mapping are shown on the right. For details, we refer readers to [67, 78]. Conformal geometric invariants can also be applied for shape analysis and recognition. Details can be found in [75].

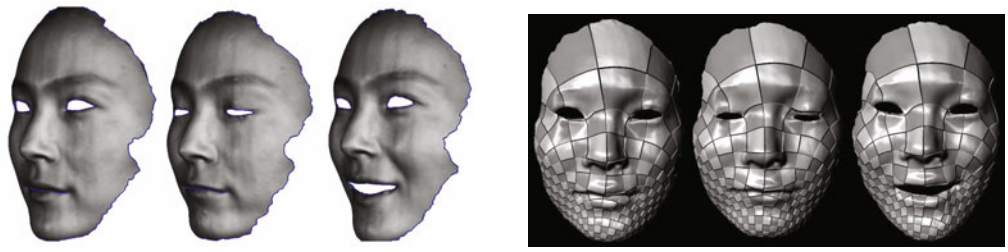

FIGURE 23. Matching among faces with different expressions.

Teichmüller theory can be applied for surface classification in [73, 42]. By using Ricci curvature flow, we can compute the hyperbolic uniformization metric. Then we compute the pants decomposition using geodesics and compute the Fenchel-Nielsen coordinates. In Figure 24, a canonical fundamental group basis

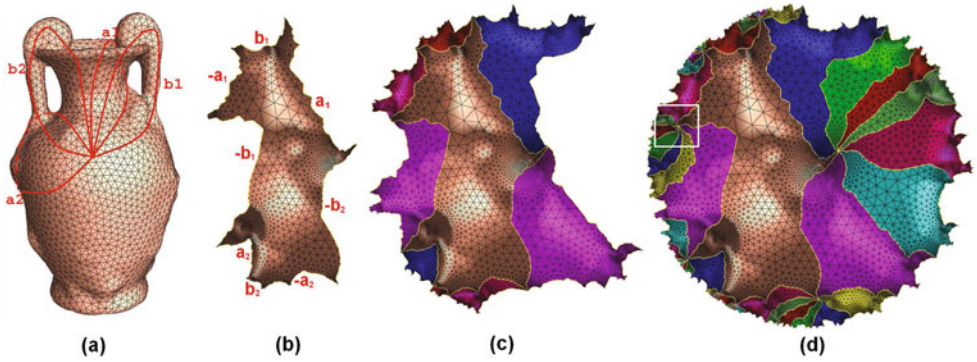

FIGURE 24. Computing finite portion of the universal covering space on the hyperbolic space.

is computed (a). Then a fundamental domain is isometrically mapped to the Poincaré disk with the uniformization metric (b). By using Fuchsian transformation, the fundamental domain is transferred (c) and a finite portion of the universal covering space is constructed in (d). Figure 25 shows the pipeline for computing the Teichmüller coordinates. The geodesics on the hyperbolic disk are found in (a), and the surface is decomposed by these geodesics (b). The shortest geodesics between two boundaries of each pair of hyperbolic pants are computed in (c), (d) and (e). The twisting angle is computed in (f). Details can be found in [42].

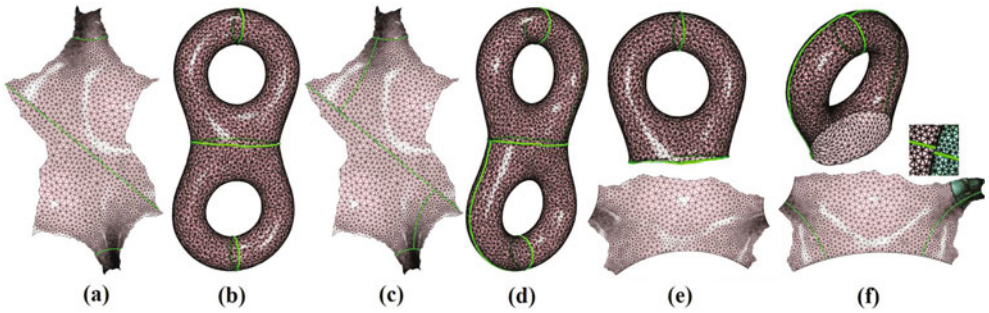

FIGURE 25. Computing the Fenchel-Nielsen coordinates in the Teichmüller space for a genus two surface.

5.5. Wireless sensor network. In the wireless sensor network field, it is important to design a Riemannian metric to ensure the delivery of packets and balance the computational load among all the sensors. Because each sensor can only collect the information in its local neighbors, it is desirable to use greedy routing. Basically, each node has virtual coordinates. The sensor sends the packet to its direct neighbor, which is the closest one to the destination. If the network has concave holes, as shown in Figure 26, the routing may get stuck at

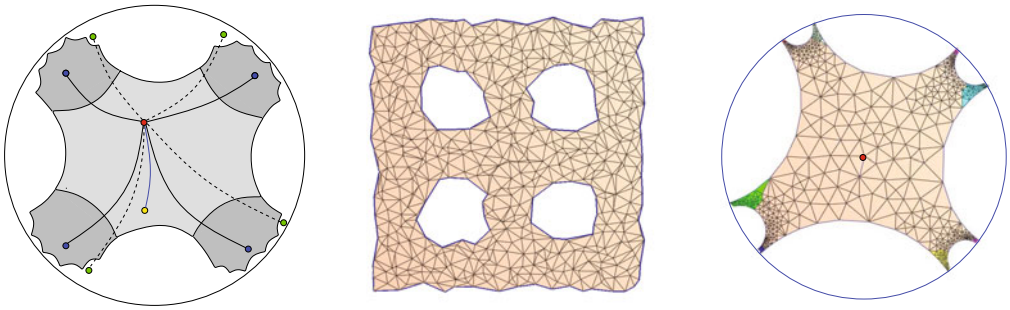

(a) Hyperbolic universal covering space

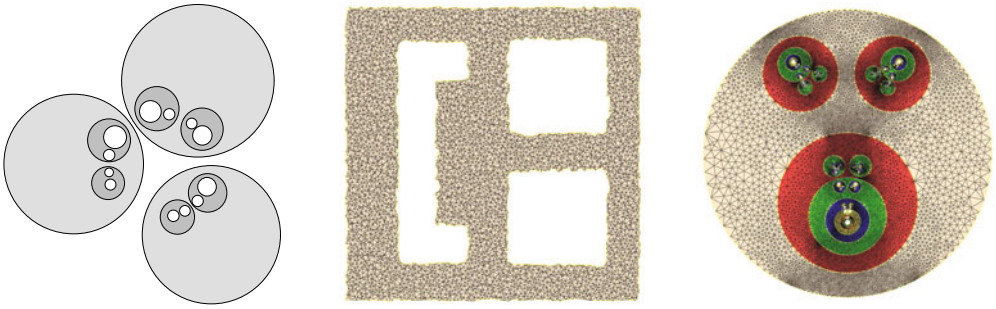

(b) Euclidean covering space

FIGURE 26. Ricci flow for greedy routing and load balancing in wireless sensor network.

the nodes along the inner boundaries. We use Ricci flow to compute the virtual coordinates, such that all inner holes become circles or hyperbolic geodesics, then greedy routing delivery is guaranteed. The delivery path is guided by geodesics under the special Riemannian metric. The covering spaces with Euclidean and hyperbolic geometry pave a new way to handle load balancing and data storage problems. Using the virtual coordinates, many shortest paths will pass through the nodes on the inner boundaries. Therefore, the nodes on the inner boundaries will be overloaded. Then, we can reflect the network about the inner circular boundaries or hyperbolic geodesics. All such reflections form the so-called Schottky group in the Euclidean case (b), or the so-called Fuchsian group in the hyperbolic case (a). We then perform the routing on the covering space. This method ensures delivery and improves load balancing using greedy routing. Implementation details can be found in [55, 76, 56].

References

1. T. Aubin, Équations differéntielles non linéaires et problème de Yamabe concernant la courbure scalaire, *J. Math. Pures Appl.* **55** no.3 (1976), 269–296.
2. L. Banjai and L. N. Trefethen, A multipole method for Schwarz-Christoffel mapping of polygon with thousands of sides, *SIAM J. Comput.* **25** no.3 (2003), 1042–1065.
3. I. Binder, M. Braverman and M. Yampolsky, On the computational complexity of the Riemann mapping, *Ark. Mat.* **45** no.2 (2007), 221–239.
4. C. J. Bishop, Conformal mapping in linear time, *Discrete Comput. Geom.* **44** no.2 (2010), 330–428.
5. A. I. Bobenko and B. A. Springborn, Variational principles for circle patterns and Koebe's theorem, *Trans. Amer. Math. Soc.* **356** (2004), 659–689.
6. A. I. Bobenko, B. A. Springborn and U. Pinkall, Discrete conformal equivalence and ideal hyperbolic polyhedra, *arXiv*:1005.2698 (2010).
7. P. L. Bowers and M. K. Hurdal, Planar conformal mapping of piecewise flat surfaces; in: H.-C. Hege et al. (eds.), *Visualization and Mathematics III*, Outgrowth of the 3rd international workshop, Berlin, Germany, May 22–25, 2002; Berlin, Springer, 2003, 3–34, 425–426; *Math. Vis.* **III** (2003), 3–34.
8. S.-S. Chern, An elementary proof of the existence of isothermal parameters on a surface, *Proc. Amer. Math. Soc.* **6** (1955), 771–782.
9. B. Chow, P. Lu and L. Ni, *Hamilton's Ricci Flow*, Amer. Math. Soc., 2006.
10. B. Chow and F. Luo, Combinatorial Ricci flows on surfaces, *J. Differential Geom.* **63** no.1 (2003), 97–129.
11. Y. Colin de Verdiére, Un principe variationnel pour les empilements de cercles, *Invent. Math.* **104** no.3 (1991), 655–669.
12. C. Costa, Example of a complete minimal immersion in $\mathbb{R}^3$ of genus one and three embedded ends, *Bol. Soc. Bras. Mat.* **15** (1984), 47–54.
13. C. Collins and K. Stephenson, A circle packing algorithm, *Comput. Geom.* **25** (2003), 233–256.
14. K. Crane, M. Desbrun and P. Schröder, Trivial connections on discrete surfaces, *Comput. Graph. Forum* **29** no.5 (2010), 1525–1533.
15. D. G. Crowdy, The Schwarz-Christoffel mapping to bounded multiply connected polygonal domains, *Proc. R. Soc. A* **461** (2005), 2653–2678.

16. D. G. Crowdy and J. S. Marshall, Conformal mappings between canonical multiply connected domains, *Comput. Methods Funct. Theory* **6** no.1 (2006), 59–76.
17. T. K. DeLillo, The accuracy of numerical conformal mapping methods: a survey of examples and results, *SIAM J. Numer. Anal.* **31** no.3 (1994), 788–812.
18. T. K. DeLillo, A. R. Elcrat and J. A. Pfaltzgraff, Schwarz-Christoffel mapping of multiply connected domains, *J. Analyse Math.* **94** no.1 (2004), 17–47.
19. M. Desbrun, M. Meyer and P. Alliez, Intrinsic parameterizations of surface meshes, *Computer Graphics Forum (Proc. Eurographics 2002)* **21** no.3 (2002), 209–218.
20. T. A. Driscoll and L. N. Trefethen, *Schwarz-Christoffel Mapping*, Cambridge Press, 2002.
21. T. A. Driscoll and S. A. Vavasis, Numerical conformal mapping using cross-ratios and Delaunay triangulation, *SIAM Sci. Comp.* **19** (1998), 1783–803.
22. H. M. Farkas and I. Kra, *Riemann Surfaces*, Graduate Texts in Mathematics **71**, Springer-Verlag, 1991.
23. M. S. Floater, Mean value coordinates, *Comput. Aided Geom. Design* **20** no.1 (2003), 19–27.
24. M. S. Floater and K. Hormann, *Surface Parameterization: a Tutorial and Survey*, Advances in Multiresolution for Geometric Modelling, **157**–**186**, Springer, 2005.
25. D. Glickenstein, Discrete conformal variations and scalar curvature on piecewise flat two and three dimensional manifolds, *arXiv*:0906.1560 (2009).
26. S. J. Gortler, C. Gotsman and D. Thurston, Discrete one-forms on meshes and applications to 3D mesh parameterization, *Comput. Aided Geom. Design* **23** no.2 (2005), 83–112.
27. C. Gotsman, X. Gu and A. Sheffer, Fundamentals of spherical parameterization for 3D meshes, *ACM Transactions on Graphics* **22** no.3 (2003), 358–363.
28. X. Gu, Y. He and H. Qin, Manifold splines, *Graphical Models* **68** no.3 (2006), 237–254.
29. X. Gu and S.-T. Yau, Global conformal parameterization, *Symposium on Geometry Processing* (2003), 127–137.
30. _____, *Computational Conformal Geometry*, Advanced Lectures in Mathematics, Vol **3**, International Press and Higher Education Press, 2007.
31. X. Gu, Y. Wang, T. F. Chan, P. M. Thompson and S.-T. Yau, Genus zero surface conformal mapping and its application to brain surface mapping, *IEEE Trans. Med. Imaging* **23** no.8 (2004), 949–958.
32. X. Gu, S. Zhang, P. Huang, L. Zhang, S.-T. Yau and R. Martin, Holoimages, *Proc. ACM Solid and Physical Modeling* (2006), 129–138.
33. R. Guo, Local rigidity of inversive distance circle packing, *Trans. Amer. Math. Soc.* **36** (2011), 4757–4778.
34. R. S. Hamilton, The Ricci flow on surfaces, in: *Mathematics and General Relativity* (Santa Cruz, CA, 1986), Contemp. Math. Amer. Math. Soc., Providence, RI, vol. **71**, 1988.
35. _____, Three manifolds with positive Ricci curvature, *J. Differential Geom.* **17** (1982), 255–306.
36. Z.-X. He and O. Schramm, Fixed points, Koebe uniformization and circle packings, *Ann. of Math.* **137** no.2 (1993), 369–406.
37. P. Henrici, *Applied and Computational Complex Analysis, Vol 3: Discrete Fourier Analysis, Cauchy Integrals, Construction of Conformal Maps, Univalent Functions*, Wiley-Interscience, 1993
38. A. N. Hirani, Discrete exterior calculus, PhD thesis, California Institute of Technology, 2003.
39. W. Hong, X. Gu, F. Qiu, M. Jin and A. E. Kaufman, Conformal virtual colon flattening, *Symposium on Solid and Physical Modeling* (2006), 85–93.
40. V. I. Ivanov and M. K. Trubetskov, *Handbook of Conformal Mapping with Computer-Aided Visualization*, CRC Press, Boca Raton, FL, 1995.

41. M. Jin, J. Kim, F. Luo and X. Gu, Discrete surface Ricci flow, *IEEE Transactions on Visualization and Computer Graphics (TVCG)* **14** no.5 (2008), 1030–1043.
42. M. Jin, W. Zeng, D. Ning and X. Gu, Computing Fenchel-Nielsen coordinates in Teichmüller shape space, *IEEE International Conference on Shape Modeling and Applications (SMI)*, 2009.
43. L. Kharevych, B. Springborn and P. Schröder, Discrete conformal mappings via circle patterns, *ACM Trans. Graph.* **25** no.2 (2006), 412–438.
44. Koebe, Kontaktprobleme der konformen Abbildung, *Ber. Sächs. Akad. Wiss. Leipzig, Math.-Phys. Kl.* **88** (1936), 141–164.
45. V. Kraevoy and A. Sheffer, Cross-parameterization and compatible remeshing of 3D models, *ACM Transactions on Graphics* **23** no.3 (2004), 861–869.
46. Y. Lai, M. Jin, X. Xie, Y. He, J. Palacios, E. Zhang, S. Hu and X. Gu, Metric-driven RoSy fields design, *IEEE Transaction on Visualization and Computer Graphics (TVCG)* **15** no.3 (2010), 95–108.
47. S. Lang, *Differential and Riemannian Manifolds*, Graduate Texts in Mathematics **160**, Springer-Verlag New York, 1995.
48. J. M. Lee and T. H. Parker, The Yamabe problem, *Bull. Amer. Math. Soc.* **17** no.1 (1987), 37–91.
49. B. Lévy, S. Petitjean, N. Ray and J. Maillot, Least squares conformal maps for automatic texture atlas generation, *SIGGRAPH 2002* (2002), 362–371.
50. F. Luo, Combinatorial Yamabe flow on surfaces, *Commun. Contemp. Math.* **6** no.5 (2004), 765–780.
51. D. E. Marshall and S. Rohde, Convergence of a variant of the zipper algorithm for conformal mapping, *SIAM J. Numer.* **45** no.6 (2007), 2577–2609.
52. C. Mercat, Discrete Riemann surfaces and the Ising model, *Comm. Math. Physics* **218** no.1 (2004), 177–216.
53. U. Pinkall and K. Polthier, Computing discrete minimal surfaces and their conjugates, *Experiment. Math.* **2** no.1 (1993), 15–36.
54. B. Rodin and D. Sullivan, The convergence of circle packings to the Riemann mapping, *J. Differential Geom.* **26** no.2 (1987), 349–360.
55. R. Sarkar, X. Yin, J.Gao and X. Gu, Greedy routing with guaranteed delivery using Ricci flows, *Proc. of the 8th International Symposium on Information Processing in Sensor Networks (IPSN'09)*, Apr, 2009, 121–132.
56. R. Sarkar, W. Zeng, J.Gao and X. Gu, Covering space for in-network sensor data storage, *Proc. of the 9th International Symposium on Information Processing in Sensor Networks (IPSN'10)*, Apr, 2010, 232–243.
57. R. Schinzinger and P. A. Laura, *Conformal Mapping: Methods and Applications*, Dover Publications, 2003.
58. R. Schoen, Conformal deformation of a Riemannian metric to constant scalar curvature, *J. Differential Geom.* **20** no.2 (1984), 479–495.
59. R. Schoen and S.-T. Yau, *Lectures on Harmonic Maps*, Conference Proceedings and Lecture Notes in Geometry and Topology, 2. Cambridge, MA, International Press, 1997, 394 p.
60. K. Stephenson, *Introduction to Circle Packing: the Theory of Discrete Analytic Functions*, Univ. Press, Cambridge, 2005.
61. G. Tewari, C. Gotsman and S. J. Gortler, Meshing genus-1 point clouds using discrete one-forms, *Comput. Graph.* **30** no.6 (2006), 917–926.
62. W. P. Thurston, *Geometry and Topology of Three-Manifolds*, Lecture Notes at Princeton University, 1980.

63. _____, *The Finite Riemann Mapping Theorem*, invited talk at the International Symposium at Purdue University on the occasion of the proof of the Bieberbach conjecture, 1985.
64. Y. Tong, P. Alliez, D. Cohen-Steiner and M. Desbrun, Designing quadrangulations with discrete harmonic forms, *Symposium on Geometry Processing* (2006), 201–210.
65. L. N. Trefethen (ed.), *Numerical Conformal mapping*, North-Holland Publishing Co., Amsterdam, 1986; reprint of *J. Comput. Appl. Math.* **14** no.1–2 (1986).
66. N. S. Trudinger, Remarks concerning the conformal deformation of Riemannian structures on compact manifolds, *Ann. Scuola Norm. Sup. Pisa* **22** no.2 (1968), 265–274.
67. S. Wang, Y. Wang, M. Jin, X. D. Gu and D. Samaras, Conformal geometry and its applications on 3D shape matching, recognition, and stitching, *IEEE Trans. Pattern Anal. Mach. Intell.* **29** no.7 (2007), 1209–1220.
68. R. Wegmann, Methods for numerical conformal mapping, in: *Handbook of Complex Analysis Vol. 2: Geometric Function Theory*, Elsevier, Amsterdam, 2005, 351–377.
69. H. Yamabe, The Yamabe problem, *Osaka Math. J.* **12** no.1 (1960), 21–37.
70. Y.-L. Yang, R. Guo, F. Luo, S.-M. Hu and X. Gu, Generalized discrete Ricci flow, *Comput. Graph. Forum* **28** no.7 (2009), 2005–2014.
71. X. Yin, J. Dai, S.-T. Yau, and X. Gu, Slit Map: conformal parameterization for multiply connected surfaces, *Geometric Modeling and Processing (GMP)* (2008), 410–422.
72. W. Zeng, M. Jin, F. Luo and X. Gu, Computing canonical homotopy class representative using hyperbolic structure, *IEEE International Conference on Shape Modeling and Applications (SMI)*, 2009.
73. W. Zeng, L. M. Lui, X. Gu, and S.-T. Yau, Shape analysis by conformal modulus, *Methods Appl. Anal.* **15** (2008), 539–556.
74. W. Zeng, F. Luo, S-T Yau and X. Gu, Surface quasi-conformal mapping by solving Beltrami equations, *IMA Conference on the Mathematics of Surfaces* (2009), 391–408.
75. W. Zeng, D. Samaras and X. Gu, Ricci Flow for 3D shape analysis, *IEEE Transaction of Pattern Analysis and Machine Intelligence (PAMI)* **32** no.4 (2010), 662–677.
76. W. Zeng, R. Sarkar, F. Luo, X. Gu and J. Gao, Resilient routing for sensor networks using hyperbolic embedding of universal covering space, *Proc. of the 29th IEEE Conference on Computer Communications (INFOCOM'10)*, Mar 15-19, 2010.
77. W. Zeng, X. Yin, M. Zhang, F. Luo and X. Gu, Generalized Koebe's method for conformal mapping multiply connected domains, *SIAM/ACM Joint Conference on Geometric and Physical Modeling (SPM)* (2009), 89–100.
78. W. Zeng, Y. Zeng, Y. Wang, X. Yin, X. Gu, and D. Samaras, 3D non-rigid surface matching and registration based on holomorphic differentials, *The 10th European Conference on Computer Vision (ECCV) 2008* (2008), 1–14.

Xianfeng David Gu E-MAIL: gu@cs.sunysb.edu
ADDRESS: *State University of New York at Stony Brook, Department of Computer Science, Stony Brook, NY 11794, U.S.A.*

Wei Zeng E-MAIL: zengwei@cs.sunysb.edu
ADDRESS: *State University of New York at Stony Brook, Department of Computer Science, Stony Brook, NY 11794, U.S.A.*

Feng Luo E-MAIL: fluo@math.rutgers.edu
ADDRESS: *Rutgers University, Department of Mathematics, Piscataway, NJ 08854, U.S.A.*

Shing-Tung Yau E-MAIL: yau@math.harvard.edu
ADDRESS: *Harvard University, Mathematics Department, Cambridge, MA 02138, U.S.A.*